

THE UNIVERSITY OF CALGARY

Power System Optimization Incorporating Hopf Bifurcations

by

Isabel Pana

A THESIS

SUBMITTED TO THE FACULTY OF GRADUATE STUDIES  
IN PARTIAL FULFILLMENT OF THE REQUIREMENTS FOR THE  
DEGREE OF MASTER OF SCIENCE

DEPARTMENT OF ELECTRICAL AND COMPUTER  
ENGINEERING

CALGARY, ALBERTA

November, 2004

© Isabel Pana 2004

**THE UNIVERSITY OF CALGARY**  
**FACULTY OF GRADUATE STUDIES**

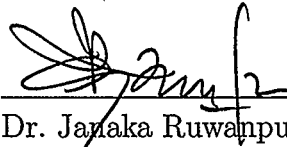
The undersigned certify that they have read, and recommend to the Faculty of Graduate Studies for acceptance, a thesis entitled "Power System Optimization Incorporating Hopf Bifurcations" submitted by Isabel Pana in partial fulfillment of the requirements for the degree of Master of Science.



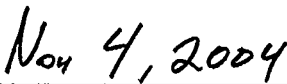
Supervisor, Dr. William D. Rosehart  
Department of Electrical and Computer Engineering



Dr. Ed Nowicki  
Department of Electrical and Computer Engineering



Dr. Janaka Ruwanpura  
Department of Civil Engineering



Date

# Abstract

The progressive increase in demand for electrical energy has driven the existing power networks towards their operational limits, as evidenced by recent major power failures. Additional new generating stations and transmission lines to the current systems are limited due to economical and environmental constraints. Therefore, operating the existing systems more efficiently, while maintaining the systems reliability, is of increasing relevance. Power systems optimization theory can be applied to improve the network operation, and is presently a topic of significant research interest.

Power networks are dynamical systems that are large, complex, and nonlinear in nature. At certain critical load values, the behavior of the system might change qualitatively. Bifurcation theory describes the nature of these changes in the system, from a stability point of view, and it has substantial importance in the study of power systems operation.

This thesis proposes the application of optimization techniques to improve the stability margin of power systems with respect to the occurrence of Hopf bifurcations. In this regard, five optimization problems are formulated in order to compute the optimal values of system variables that yield the maximum system loadability. The effectiveness of the proposed optimization problems is validated using two test systems, and a comparative analysis is presented based on their performance, initialization requirements and assumption of the loading direction.

## Acknowledgments

I would like to express my thanks to my supervisor Dr. Bill Rosehart for the guidance and constructive advice he has provided. Additional thanks are extended to my committee members Dr. Ed Nowicki for his continual support and encouragement and Dr. Janaka Ruwanpura for his comments and suggestions.

I deeply appreciate the assistance I received from Dr. Karrari and Dr. Malik, and enjoyed the discussions with Tamer, Hong and Wael in power research group. I specially would like to thank Tony for all his help and interesting discussions we had. I also acknowledge all the help from the staff at the Graduate Studies and the Electrical and Computer Engineering Department.

I would like to thank my friends, Hilary, Peng, Codruta, Dr. Mehran, Behrokh and all others for being patient and supportive. My deepest gratitude is for my family, without their help and support I could hardly complete this thesis. Finally, my special thanks are for Fabio, no words can express my appreciation for all that you have done.

This work is dedicated to Bernardo Pana

# Table of Contents

Approval Page	ii
Abstract	iii
Acknowledgments	iv
Table of Contents	vi
<b>1 Introduction</b>	<b>1</b>
1.1 Background . . . . .	1
1.2 Literature Review . . . . .	2
1.3 Research Motivation and Objectives . . . . .	5
1.4 Implementation Methods . . . . .	7
1.5 Thesis Organization . . . . .	8
<b>2 System Modeling</b>	<b>11</b>
2.1 Introduction . . . . .	11
2.2 Power Flow Equations . . . . .	11
2.2.1 Load Power . . . . .	13
2.2.2 Branch Power . . . . .	15
2.3 Load Tap Changing (LTC) Transformer . . . . .	17
2.4 Induction Machine . . . . .	19
2.4.1 Introduction . . . . .	19
2.4.2 Slip and Operating Conditions . . . . .	20
2.4.3 Synchronously Rotating Reference Frame Transformation . . . . .	21
2.4.4 Machine Model in the Synchronously Rotating “ $qd0$ ” Reference Frame . . . . .	24
2.4.5 Torque Equation . . . . .	27
2.5 Complete Model of the System . . . . .	29
2.6 Summary . . . . .	30
<b>3 Power System Instability and Bifurcations</b>	<b>31</b>
3.1 Introduction . . . . .	31
3.2 Small-disturbance Power System Stability Analysis . . . . .	32
3.3 Bifurcation Theory . . . . .	36
3.3.1 Saddle-Node Bifurcations (SNB) . . . . .	37
3.3.2 Hopf Bifurcations . . . . .	38

3.4	Methods to Detect Bifurcations . . . . .	40
3.4.1	Singular Value and Eigenvalue indices . . . . .	40
3.4.2	Continuation Method . . . . .	42
3.5	Optimal Power Flow (OPF) . . . . .	45
3.6	Summary . . . . .	47
<b>4</b>	<b>Optimal Power Flow with Hopf Bifurcation Constraints</b>	<b>49</b>
4.1	Introduction . . . . .	49
4.2	Generalized Eigenvalue Problem . . . . .	50
4.3	Optimization of the Maximum System Loadability (MSL) with Respect to Hopf Bifurcations . . . . .	52
4.3.1	Generalized Eigenvalue Based Hopf Bifurcation Constrained Optimal Power Flow (GEHB-OPF) Problem . . . . .	54
4.3.2	Critical Eigenvalue Based Hopf Bifurcation Constrained Optimal Power Flow (CEHB-OPF) Problem . . . . .	58
4.3.3	Stability Constrained Optimal Power Flow (S-OPF) Problem . . . . .	60
4.4	Optimization of a Hopf Bifurcation Index . . . . .	61
4.4.1	Eigenvalue Index Optimization problem . . . . .	62
4.4.2	Singular Value Index Optimization problem . . . . .	63
4.5	Summary . . . . .	65
<b>5</b>	<b>Numerical Analysis</b>	<b>67</b>
5.1	Introduction . . . . .	67
5.2	Effect of the Controllable Parameters in the Loading Margin of the 3-Bus Test System . . . . .	68
5.3	Results of the Optimization Problems . . . . .	72
5.3.1	Generalized Eigenvalue Based HB Constrained OPF (GEHB-OPF) Problem . . . . .	72
5.3.2	Critical Eigenvalue Based HB Constrained OPF Problem (CEHB-OPF) . . . . .	77
5.3.3	Stability Constrained OPF Problem (S-OPF) . . . . .	80
5.3.4	EVI Optimization Problem . . . . .	82
5.3.5	SVI Optimization Problem . . . . .	89
5.4	Comparison of Formulations . . . . .	93
5.5	Summary . . . . .	95
<b>6</b>	<b>Conclusion</b>	<b>96</b>
<b>A</b>	<b>Solution of Linear Ordinary Differential Equations with Constant Coefficients</b>	<b>99</b>





## List of Tables

5.1	Optimization results for the ‘3-bus’ test system, when solving the GEHB-OPF problem . . . . .	74
5.2	Optimization results for the ‘3-bus’ test system, when solving the CEHB-OPF problem . . . . .	78
5.3	Optimization results for ‘IEEE14bus’ test system, when solving the CEHB-OPF problem . . . . .	79
5.4	Optimization results for the ‘3-bus’ test system, when solving the S-OPF problem . . . . .	81
5.5	Optimization results for the ‘IEEE14bus’ test system, when solving the S-OPF problem . . . . .	82
5.6	Optimization results for the ‘3-bus’ test system, when solving the EVI optimization problem . . . . .	84
5.7	Maximum loadability of the system and the corresponding critical eigenvalue, ‘3-bus’ test system, when solving the EVI optimization problem, . . . . .	84
5.8	Maximum loadability of the system and the corresponding critical eigenvalue, ‘IEEE14bus’ test system, when solving the EVI optimization problem . . . . .	86
5.9	Optimization results for the ‘IEEE14bus’ test system, when solving the EVI optimization problem . . . . .	87
5.10	Maximum loadability of the system with the corresponding critical eigenvalue, ‘3-bus’ test system, when solving the SVI optimization problem, . . . . .	90
5.11	Optimization results for the ‘3-bus’ test system, when solving the SVI optimization problem . . . . .	90
5.12	Maximum loadability of the system with the corresponding critical eigenvalue, ‘IEEE14bus’ test system, when solving the SVI optimization problem . . . . .	91
5.13	Optimization results for ‘IEEE14bus’ test system , when solving the SVI optimization problem . . . . .	91
5.14	Comparison of maximum loading parameter, loading margin improvement, and number of iterations to converge, in all five optimization problem formulations. The test system used is the 3-bus test system.	94

5.15	Comparison of maximum loading parameter, loading margin improvement, and number of iterations to converge, in all five optimization problem formulations. The test system used is the 14-bus test system. No results were obtained for the GEHB-OPF, since the optimization procedure did not converge. . . . .	95
------	---	----

## List of Figures

2.1	Illustration of the power transfer through a LTC transformer. (a) LTC transformer model. (b) The complex terminal power, denoted by $S_{ltc(k)}$ , is transferred from the primary to the secondary side of the $k^{\text{th}}$ LTC transformer [33]. . . . .	18
2.2	Relationship between stator and rotor $abc$ -axes and synchronously rotating “ $qd0$ ” reference frame [35]. . . . .	23
3.1	Example of a bifurcation diagram showing saddle-node bifurcation, where $z$ is typically a load bus voltage magnitude in power systems . . . . .	37
3.2	A complex conjugate pair of purely imaginary eigenvalues crossing the imaginary axis . . . . .	39
3.3	Bifurcation diagram obtained by continuation method . . . . .	43
5.1	Schematic diagram of the 3-bus test system . . . . .	67
5.2	Schematic diagram of 14-bus test system [54] . . . . .	68
5.3	The maximum loading parameter $\lambda$ as a function of the voltage reference of the LTC transformer ( $V_{\text{ref}}$ ) and the slack bus voltage ( $V_{\text{slack}}$ ) for the ‘3-bus’ test system. . . . .	70
5.4	The maximum loading parameter $\lambda$ as a function of the slack bus voltage ( $V_{\text{slack}}$ ) for the ‘3-bus’ test system. The reference voltage of the LTC transformer is fixed at 1.0 P.U. . . . .	70
5.5	The maximum loading parameter $\lambda$ as a function of the voltage reference of the LTC transformer ( $V_{\text{ref}}$ ) for the ‘3-bus’ test system. The slack bus voltage is fixed at 1.0 P.U. . . . .	71
5.6	Voltage profile of bus 2 in the 3-bus test system, when solving the GEHB-OPF problem. The lower curve indicates the original system and the upper curve represents the optimal system. Bifurcation points are shown for each profile . . . . .	75
5.7	Eigenvalue movement in the complex plain, ‘3-bus’ test system, when solving the GEHB-OPF . . . . .	75
5.8	Enlargement of the HB region, ‘3-bus’ test system, when solving the GEHB-OPFs . . . . .	76
5.9	Voltage profile of bus 13 in the ‘IEEE14bus’ test system, when solving the CEHB-OPF problem. The lower curve indicates the original system and the upper curve represents the optimal system . . . . .	79
5.10	Enlargement of the HB region, ‘IEEE14bus’ test system, when solving the CEHB-OPF problem . . . . .	80

5.11	Enlargement of the HB region, ‘3-bus’ test system, when solving the EVI optimization problem. Arrows indicate the movement of the two purely real eigenvalues which eventually collide and form a complex conjugate pair. As the value of $\lambda$ increases the pair move towards the imaginary axis. The point where the complex conjugate pair reach the imaginary axis is shown by circles . . . . .	85
5.12	Voltage profile of bus 2 in the ‘3-bus’ test system, when solving the EVI optimization problem, . . . . .	87
5.13	Voltage profile of bus 13 in the ‘IEEE14bus’ test system, when solving the EVI optimization problem. The lower profile represents the system with the optimal values of the controllable parameters and the upper profile is for the original system. The dashed line is used to show the lower voltage limit . . . . .	88
5.14	Enlargement of the HB region, ‘IEEE14bus’ test system, when solving the EVI optimization problem. Arrows indicate the movement of the two purely real eigenvalues which eventually crosses the imaginary axis as the value of $\lambda$ increases . . . . .	89
5.15	Voltage profile of bus 2 in the ‘3-bus’ test system, when solving the SVI optimization problem, . . . . .	92
5.16	Voltage profile of bus 13 in the ‘IEEE14bus’ test system, when solving the SVI optimization problem, the lower curve indicates the original system and the upper curve represents the optimal system . . . . .	92

## List of Symbols and Acronyms

### Symbols:

$\mathbf{F}(\cdot)$	:	Set of differential equations used to model the system
$\mathbf{G}(\cdot)$	:	Set of algebraic equations used to model the system
$D$	:	Number of differential variables
$A$	:	Number of algebraic variables
$CP$	:	Number of controllable parameters
$N$	:	Number of system nodes (or buses)
$\mathbf{x}$	:	Vector of system dynamic (or state) variables
$\mathbf{y}$	:	Vector of system algebraic variables
$\lambda$	:	Loading parameter (or loading factor),
$\mathbf{p}$	:	Vector of system controllable parameters
$\psi_{qs}$	:	Stator flux linkage per second along the $q$ -axis
$\psi_{ds}$	:	Stator flux linkage per second along the $d$ -axis
$\psi_{qr}$	:	Rotor flux linkage per second along the $q$ -axis
$\psi_{dr}$	:	Rotor flux linkage per second along the $d$ -axis
$\omega_r$	:	Rotor angular speed
$a$	:	tap setting of the load tap changing transformer
$V_{\text{ref}}$	:	Reference voltage of load tap changing transformer
$v_{qs}$	:	Stator voltage along the $q$ -axis
$v_{ds}$	:	Stator voltage along the $d$ -axis
$P_m$	:	Active power consumed by the induction motor
$Q_m$	:	Reactive power consumed by the induction motor

$V_R$	:	Real component of the bus voltage
$V_I$	:	Imaginary component of the bus voltage
$\mathbf{P}_{\text{gen}}$	:	Vector of active power generation in the system
$\mathbf{Q}_{\text{gen}}$	:	Vector of reactive power generation in the system
$\mathbf{J}$	:	Jacobian matrix of the system
$\mathbf{J}_{\text{reduced}}$	:	Reduced Jacobian matrix of the system
$\eta$	:	eigenvalue
$\alpha$	:	Real component of the eigenvalue
$\beta$	:	Imaginary component of the eigenvalue
$\sigma$	:	Singular value
$\mathbf{v}$	:	Eigenvector associated with the eigenvalue $\eta$

### Acronyms:

LTC	:	Load Tap Changing
P.U.	:	Per Unit
DAE	:	Differential-Algebraic Equations
HB	:	Hopf Bifurcation
SNB	:	Saddle-Node Bifurcation
MSL	:	Maximum System Loadability
OPF	:	Optimal Power Flow
GEHB-OPF	:	Generalized Eigenvalue Based Hopf Bifurcation Constrained OPF

CEHB-OPF	:	Critical Eigenvalue Based Hopf Bifurcation Constrained OPF
S-OPF	:	Stability Constrained OPF
EVI	:	Eigenvalue Index OPF
SVI	:	Singular Value Index OPF
NR	:	Newton-Raphson method
SNR	:	Sequential Newton-Raphson method
SQP	:	Sequential Quadratic Programming

# Chapter 1

## Introduction

### 1.1 Background

The progressive increase in demand for electrical energy has driven the existing power networks towards their operational limits, as evidenced by recent major power failures [1]. Additional new generating stations and transmission lines to the current systems, are limited due to economical and environmental constraints [2, 3]. Therefore, operating the existing systems more efficiently, while maintaining the systems reliability, is of increasing relevance. Power systems optimization theory can be applied to improve the network operation, and is presently a topic of significant research interest [4].

Power networks are dynamical systems that are large, complex, and nonlinear in nature. A power system must be operated at a stable equilibrium point, and this operating point varies smoothly with gradual changes in the system parameters. Normally, the parameter of interest in such analysis is the system loading level [5]. At certain critical load values, the behavior of the system might change qualitatively [5]. Bifurcation theory describes the nature of these changes in the system, from a stability point of view [6], and it has substantial importance in the study of power systems operation.

Highly stressed power systems can thus be limited, in their generation and transmission capabilities, by the occurrence of bifurcation. Therefore, network optimiza-



tion requires the incorporation of bifurcation phenomena as a limiting factor. Two important types of bifurcation arising in power systems are the saddle-node and Hopf bifurcations [7]. Saddle-node bifurcation occurs at a loading level such that no equilibrium solution can be found with further increases in the load. Hopf bifurcation is characterized by the emergence of oscillatory behavior in the network when the load is increased beyond a critical value.

## 1.2 Literature Review

Voltage collapse and oscillatory instability problems, arising by slow variation of a system parameter, are inherently nonlinear phenomena that can be studied by bifurcation theory [8]. Voltage collapse is an instability problem associated with heavily loaded power systems that lead to abnormally low voltages in a significant part of the network and blackout [9]. Voltage instability problems can be related to saddle-node bifurcations [5], during which the system equilibrium disappears as the load is gradually increased.

Hopf bifurcation (also known as oscillatory bifurcation) occurs when a pair of complex conjugate eigenvalues of the system matrix crosses the imaginary axis of the complex plane, causing oscillations in the system [10]. It has been observed that the interaction between the dynamics of induction motors and tap changing transformers can cause oscillatory problems related to the Hopf bifurcation in a power system [11].

Substantial research has been conducted to analyze the mechanism of occurrence of both saddle-node and Hopf bifurcations in power systems. In [12], the authors

studied qualitative changes in the behavior of a simple, three bus power network, as the load is increased. They reported oscillatory problems in the system prior to voltage collapse and observed that the approximate frequency of oscillation was related to the imaginary part of the largest complex eigenvalues of the system Jacobian matrix linearized about the operating point. In [7], an introduction to bifurcation theory and the application of this theory to analyze a three bus power system is presented. It is shown that as the power consumption of the load is varied the system experiences first a Hopf bifurcation and then a saddle-node bifurcation. The authors in [13] provide a detailed definition, classification and analysis of voltage-collapse phenomena using bifurcation theory. They showed that voltage collapse is directly related to the occurrence of saddle-node bifurcation in a modeled power system. Furthermore, they have indicated that their model can be extended by including dynamics of voltage control devices such as tap changing transformers to reveal other kinds of system instabilities including Hopf bifurcations. In [14], the qualitative behavior of power system dynamics as modeled by differential-algebraic equations is discussed. The authors have emphasized on the importance of studying Hopf bifurcations as it has been shown that the stability of the system equilibrium can be lost before reaching the point of collapse. They have concluded that Hopf bifurcation can be the initial event leading to a system failure. In [15], the dynamics of a general power system is represented by a parameter-dependent differential-algebraic model and local bifurcations such as Hopf and saddle-node bifurcations are discussed. In [16], the Hopf bifurcation theorem is used to study low frequency oscillations in a three bus power network. In all the mentioned papers, simple examples are used to demonstrate the application of bifurcation theory in power systems. However, in [17] the authors

present a detailed bifurcation analysis of real multiparameter power systems using the southern section of the Brazilian network to demonstrate that the basic concepts can be applied to large power networks as well.

It is important to anticipate the development of an impending bifurcation in a heavily loaded power network, so that effective action can be taken to avoid system instability. Hence, several methods have been developed to detect and predict the occurrence of Hopf bifurcations. The authors in [18] have analyzed the occurrence of Hopf bifurcation in the July 1992 disturbance on the mid-western segment of the US interconnection system, and proposed an iterative algorithm for the computation of the Hopf bifurcation. In [19], several indices are proposed, for on-line applications, to detect and predict oscillatory instabilities associated with the occurrence of Hopf bifurcations in power systems. These indices are based on the minimum singular value of the modified system matrix. The distance to the closest Hopf or saddle-node bifurcation, with respect to a slow varying system parameter (e.g. load), can be computed using a continuation method as shown in [20]. However, the direction of the load increase should be known in this method. Furthermore, this method cannot be used if there is more than one parameter that drives the system to bifurcation (e.g., several loads changing independently of each other). The authors in [21] have proposed an optimization based method to indicate the closest Hopf bifurcation in a three bus test system, assuming that the controllable network parameters are fixed and the multiple loads are varied independently.

Several studies have been performed regarding the control of oscillatory problems in a power network. The authors in [22] have compared the application of power system stabilizers (PSS) and flexible AC transmission systems (FACTS) devices to

control system oscillations. They have shown that FACTS controllers, such as static Var Compensators (SVC) or shunt static synchronous compensators (STATCOM), have an advantage over PSS controllers, as they can increase the system stability margin by improving the system voltage profile. However, FACTS controllers are expensive solutions. Another important aspect of using FACTS controllers to effectively damp system oscillation is the controllers location in power network. Although the authors have proposed a method based on eigenvalue analysis to identify the best location, the placement of the controller in those locations might not correspond to the increase in the system loadability. The authors in [23] proposed a method to determine the optimal load curtailment in order to improve the stability margin of the system, based on a sensitivity analysis of the distance to bifurcation. However, actions based on their method is not always possible, since some important loads can be shed only in emergency situations. In [24, 25] the author formulates an optimization problem to compute controllable parameters of a power system such that the distance to a saddle-node bifurcation is maximized. However, oscillatory instabilities, that can occur well before a system reaches its collapse point, are neglected.

### 1.3 Research Motivation and Objectives

Theoretical studies and computational simulations of power systems have demonstrated that the occurrence of Hopf bifurcations can lead to instability in heavily loaded networks. These instability problems have also been observed in practice, as evidenced by recent power failures, e.g., the August 1996 power outage in the western states of USA and south of Canada [26].

The management of system oscillations in a power network is accomplished through a combination of planning and controlling actions:

- Controlling measures to handle Hopf bifurcation are intended to hinder an imminent Hopf bifurcation, or lessen its effects on the system operation. Such control actions include load shedding, and employment of PSS and FACTS controllers.
- Planning measures are related to the power network design. The maximization of the stability margin of the system is a design objective in the delineation of a new system, or in the optimization of an existing system's capability.

The goal of this thesis is to investigate how to improve the system stability margin with respect to the occurrence of Hopf bifurcations, through the application of optimization techniques. In this regard, a proper system modeling to reveal oscillatory instabilities is essential, and a complete power system model represented by a set of differential and algebraic equations (DAE) is employed in the thesis.

The main objectives of the present research are as follows:

- Development of optimal power flow formulations to directly maximize the system loadability with respect to the occurrence of Hopf bifurcations. The conditions that describe the Hopf bifurcation are added as constraints in these optimization formulations.
- Development of optimal power flow formulations to maximize indices that represent an indirect measure of the distance to the occurrence of Hopf bifurcations. In this case, the conditions that mathematically describe the Hopf bifurcation are not considered as constraints of the optimization problems.

- Incorporation of the dynamics of transformer tap changers and fifth order induction motors into the classical optimal power flow problem.
- Implementation of the proposed formulations. Tests are conducted to evaluate the effectiveness of the proposed techniques in the improvement of the loading margin of the system, as well as to gain a better understanding of the limitations of the proposed methods.

## 1.4 Implementation Methods

The initial solution of the optimization problems is obtained using a sequential Newton-Raphson method, implemented in Matlab. All the optimization problems formulated in this thesis are solved using the optimization routines in the Matlab optimization toolkit, with the exception of the Generalized Eigenvalue Based Hopf Bifurcation Constrained Optimal Power Flow problem (GEHB-OPF problem, to be described in Section 4.1), which is implemented in AMPL [27].

The AMPL modeling language allows the development of optimization problems, and the application of optimization solver packages to search for the optimal solution of a given problem. The solver LOQO [28], which is based on the Nonlinear Logarithmic Barrier Interior Point method [29], is employed in solving the GEHB-OPF problem. The AMPL language, however, does not permit the implementation of optimization problems that require the explicit computation of the eigenvalues or the singular values of the system matrix. Therefore, the remaining optimization problems are implemented in Matlab, whose solver is based on the Sequential Quadratic Programming method [30].

A continuation method is implemented in Matlab to obtain the distance to bifurcation for both the original and the optimal sets of controllable parameters. Furthermore, the continuation method routine provides the data for plotting bifurcation diagrams and graphs depicting the eigenvalues movement in the complex plane. These plots are necessary for the analysis of the proposed optimization problems.

## 1.5 Thesis Organization

The thesis is organized as follows:

- Chapter 2** establishes a mathematical model suitable to perform power systems stability analysis with respect to the Hopf bifurcations. The dynamical behavior of a power system is described by a set of differential and algebraic equations. These equations are formed using mathematical model of a fifth order induction motor, a load tap changing (LTC) transformer, and power flow equations.
- Chapter 3** provides concise explanation on small-disturbance system stability analysis of the modeled power system. The differential-algebraic model of the system is linearized around an operating point of interest. The eigenvalues of the linearized model are used to determine the stability characteristic of the power system. Bifurcation theory along with two typical types of bifurcations (i.e. saddle-node and Hopf bifurcations) are briefly explained. Methods to predict and detect bifurcations are subsequently presented. The application of optimization theory for power system stability analysis is demonstrated

using the traditional optimal power flow problem.

**Chapter 4** presents the research contributions of this thesis. The traditional optimal power flow problem is modified to incorporate the algebraic and differential equations of induction motors and LTC transformers, as well as the critical eigenvalue or singular value of the generalized eigenvalue problem. This modification is necessary in order to include the stability constraints with respect to the Hopf bifurcations in the OPF problem. Two approaches are proposed to increase the stability margin of a given power system. One approach is to directly maximize the system loading margin with respect to the occurrence of Hopf bifurcations. In this method, the mathematical conditions defining the bifurcation point are explicitly modeled. The other approach is to use an indirect measure of the distance to the Hopf bifurcation as the objective function to be maximized. Within these approaches five novel optimization problems are formulated and discussed. The advantage and disadvantage of each problem is presented.

**Chapter 5** presents and discusses the results obtained from applying the proposed optimization problems to two test systems. A three bus test system is used to demonstrate the basic concepts and highlight the main issues. A 14 bus test system is also used to study the performance of the problems when applied to larger systems. For the three bus test system, an exhaustive search of the optimal controllable parameters is performed to study the effects of these parameters



in increasing the loading margin. A detailed comparison of formulations with respect to their performance, initialization requirements, effectiveness and loading direction assumption is given.

**Chapter 6** summarizes the research performed in this thesis. The main contributions of the research are highlighted. A discussion on potential future investigations regarding the optimization of the maximum loadability of power systems with respect to Hopf bifurcations is included.

# Chapter 2

## System Modeling

### 2.1 Introduction

A typical power system network is comprised of loads, generators, and various control devices interconnected by transmission lines. A mathematical model of a power system may consist of a set of differential and algebraic equations representing the modeling of the system's components and the balance of power among them.

This chapter presents a mathematical model used to perform power systems stability analysis in order to study Hopf bifurcations. A brief discussion is given on the mathematical models of the system components, including induction motors and load tap changing (LTC) transformers. Power flow equations in rectangular coordinates are also presented.

Throughout this work, the system variables are expressed in per unit system to simplify the analysis by eliminating the units. Per unit quantities are normalized by their base values.

### 2.2 Power Flow Equations

The study of a power systems in steady-state operation is referred to as power flow analysis [31]. Power flow analysis use a set of algebraic equations (power flow equations), to determine the voltages at each bus as well as the active and reactive power

flowing into each line in a power system, under a given set of load conditions.

Power flow equations represent the active and reactive power balance at each bus (or node) in the network. Let  $N$  be the total number of buses in a system, and  $i$  indicates a particular bus or node in that system. Then, the difference between the power generated at bus  $i$  and the power consumed by the load at that bus (i.e. local load) equals the power flow into the branches connected to the bus  $i$ , as shown in the following equations:

$$0 = P_{\text{gen}(i)} - P_{\text{load}(i)} - P_{\text{branch}(i)} - \sum_{k=1}^T e_{ik} P_{\text{lrc}(k)} \quad (2.1)$$

$$0 = Q_{\text{gen}(i)} - Q_{\text{load}(i)} - Q_{\text{branch}(i)} - \sum_{k=1}^T e_{ik} Q_{\text{lrc}(k)} \quad (2.2)$$

where:

- $P_{\text{gen}(i)}$  and  $Q_{\text{gen}(i)}$  are the active and reactive power generated at bus  $i$  respectively;
- $P_{\text{load}(i)}$  and  $Q_{\text{load}(i)}$  are the active and reactive power absorbed by the loads connected at the bus  $i$ , as discussed in Section 2.2.1;
- $P_{\text{branch}(i)}$  and  $Q_{\text{branch}(i)}$  are defined as the active and reactive power leaving the  $i^{\text{th}}$  bus, through transmission lines;
- $T$  is the number of the LTC transformers in the network
- $\mathbf{E} = [e_{i,k}]$  is the LTC connection matrix, that describes the connection between

each LTC transformer and the bus to which it is attached, as follows:

$$e_{i,k} = \begin{cases} 1, & \text{if the primary side of LTC } k \text{ is connected to the bus } i; \\ -1, & \text{if the secondary side of LTC } k \text{ is connected to the bus } i; \\ 0, & \text{otherwise.} \end{cases}$$

- $P_{\text{ltc}(k)}$  and  $Q_{\text{ltc}(k)}$  are the active and reactive power being transferred from the primary side to the secondary side of the  $k^{\text{th}}$  LTC transformer (assuming a lossless transformer).

If there is no generator at bus  $i$  then  $P_{\text{gen}(i)}$  and  $Q_{\text{gen}(i)}$  are set to zero in (2.1) and (2.2). Otherwise, it is assumed that  $P_{\text{gen}(i)}$  is a pre-specified parameter of the network in all generator buses, except the slack bus [31]. The slack bus is a generator bus where the active generated power is not scheduled. Therefore, any mismatch between the active generated and consumed power in the network is balanced by the active power of the slack bus.

The slack bus also serves as an angle reference for the network. It is usual to assume that the voltage angle of the slack bus is zero. Equivalently, in rectangular coordinates, a zero voltage angle corresponds to fixing the imaginary component of the voltage at zero.

In this work, generator dynamics are neglected, therefore, steady-state voltage sources are used to represent generators.

### 2.2.1 Load Power

In the present work, the loading elements of the network are categorized as follows:

- **Constant power load:** the active and reactive power consumed by the load are pre-specified and are not a function of frequency or voltage. The total active and reactive power absorbed by the constant power loads connected to bus  $i$  are denoted by  $P_{c(i)}$  and  $Q_{c(i)}$  respectively.
- **Induction motors:** the active and reactive power consumed by the  $k^{\text{th}}$  induction motor are denoted by  $P_{m(k)}$  and  $Q_{m(k)}$ , respectively. These quantities are dependent on the amount of mechanical load connected to the motor and the terminal voltage, and will be discussed in greater detail in Section 2.4.

The total power absorbed at the bus  $i$  is the sum of the power consumed by the constant power load and the induction motors at that bus, given by:

$$P_{\text{load}(i)} = P_{c(i)} + \sum_{k=1}^M c_{ik} P_{m(k)} \quad (2.3)$$

$$Q_{\text{load}(i)} = Q_{c(i)} + \sum_{k=1}^M c_{ik} Q_{m(k)} \quad (2.4)$$

where

- $M$  is the number of the induction motors in the network, and
- $\mathbf{C} = [c_{i,k}]$  is the induction machine connection matrix, which describes the connection between each induction motors and the bus to which it is attached. It is defined as:

$$c_{i,k} = \begin{cases} 1, & \text{if machine } k \text{ is connected to the bus } i; \\ 0, & \text{otherwise.} \end{cases}$$

### 2.2.2 Branch Power

It is necessary to define the notation for elements of the nodal analysis in order to present the branch power equations. Let  $\hat{G}_{ik}$  and  $\hat{B}_{ik}$  be the conductance and the susceptance between the nodes  $i$  and  $k$ , for  $i \neq k$ . The conductance and susceptance between node  $i$  and the ground are denoted by  $\hat{G}_{ii}$  and  $\hat{B}_{ii}$ , respectively. The line conductances and susceptances are computed as:

$$\hat{G}_{ik} = \frac{r_{ik}}{r_{ik}^2 + x_{ik}^2} \quad \text{and} \quad \hat{B}_{ik} = \frac{-x_{ik}}{r_{ik}^2 + x_{ik}^2}$$

where  $r_{ik}$  and  $x_{ik}$  are the resistance and reactance of the transmission line between the buses  $i$  and  $k$ , accordingly. If  $i = k$ , then  $r_{ii}$  and  $x_{ii}$  are the resistance and reactance between bus  $i$  and the ground.

For transformers, let  $t_{ik}$  be the tap setting of the fixed tap transformer placed in the transmission line connecting buses  $i$  and  $k$ , where  $i$  is the sending bus and  $k$  is the receiving bus. When there is no transformer between buses  $i$  and  $k$ , it is convenient to assume the existence of a transformer whose fixed tap ratio is given by  $t_{ik} = 1$ . In this case, bus  $i$  and  $k$  are also regarded as the sending and receiving buses, respectively.

The conductance matrix  $\mathbf{G} = [G_{ik}]$  is then given by:

$$\begin{aligned} G_{ii} &= \sum_{\substack{j=1 \\ i \text{ sending} \\ j \text{ receiving}}}^N t_{ij}^2 \hat{G}_{ij} + \sum_{\substack{j=1 \\ i \text{ receiving} \\ j \text{ sending}}}^N \hat{G}_{ij} \\ G_{ik} &= -t_{ik} \hat{G}_{ik}, \quad i \neq k \end{aligned}$$

where  $i \in \{1, 2, \dots, N\}$ ,  $k \in \{1, 2, \dots, N\}$ , and  $N$  is the total number of buses in

the system. Analogously, the susceptance matrix  $\mathbf{B} = [B_{ik}]$  is then given by:

$$\begin{aligned} B_{ii} &= \sum_{\substack{j=1 \\ i \text{ sending} \\ j \text{ receiving}}}^N t_{ij}^2 \hat{B}_{ij} + \sum_{\substack{j=1 \\ i \text{ receiving} \\ j \text{ sending}}}^N \hat{B}_{ij} \\ B_{ik} &= -t_{ik} \hat{B}_{ik}, \quad i \neq k \end{aligned}$$

The active power  $P_{\text{branch}(i)}$  and the reactive power  $Q_{\text{branch}(i)}$  leaving the  $i^{\text{th}}$  bus are derived as follows. Denote by  $V_{\text{R}(i)}$  and  $V_{\text{I}(i)}$  the real and imaginary components of the voltage at bus  $i$  respectively. Define the following complex quantities, in rectangular coordinates:

- $V_{(i)} = V_{\text{R}(i)} + jV_{\text{I}(i)}$  is the complex voltage at bus  $i$ ,
- $I_{(i)} = I_{\text{R}(i)} + jI_{\text{I}(i)}$  is the net complex current at bus  $i$ , and
- $Y_{ik} = G_{ik} + jB_{ik}$  is the  $(i, k)$  element of the admittance matrix  $\mathbf{Y} = \mathbf{G} + j\mathbf{B}$ .

The vector  $\mathbf{I}$  of complex currents can be obtained from the vector  $\mathbf{V}$  of complex voltages as:

$$\begin{aligned} \mathbf{I} &= \mathbf{I}_{\text{R}} + j\mathbf{I}_{\text{I}} = \mathbf{Y}\mathbf{V} \\ &= (\mathbf{G} + j\mathbf{B})(\mathbf{V}_{\text{R}} + j\mathbf{V}_{\text{I}}) \\ &= (\mathbf{G}\mathbf{V}_{\text{R}} - \mathbf{B}\mathbf{V}_{\text{I}}) + j(\mathbf{G}\mathbf{V}_{\text{I}} + \mathbf{B}\mathbf{V}_{\text{R}}) \end{aligned}$$

Therefore, the real and imaginary components of the current at bus  $i$  are written as:

$$\begin{aligned} I_{\text{R}(i)} &= \sum_{k=1}^N G_{ik} V_{\text{R}(k)} - \sum_{k=1}^N B_{ik} V_{\text{I}(k)} \\ I_{\text{I}(i)} &= \sum_{k=1}^N G_{ik} V_{\text{I}(k)} + \sum_{k=1}^N B_{ik} V_{\text{R}(k)} \end{aligned} \tag{2.5}$$

The apparent power  $S_{\text{branch}(i)}$  flowing into the branches connected to bus  $i$  is given by:

$$\begin{aligned}
 S_{(i)} &= P_{(i)} + jQ_{(i)} = V_{(i)} I_{(i)}^* \\
 &= (V_{R(i)} + jV_{I(i)})(I_{R(i)} - jI_{I(i)}) \\
 &= (V_{R(i)} I_{R(i)} + V_{I(i)} I_{I(i)}) + j(V_{I(i)} I_{R(i)} - V_{R(i)} I_{I(i)})
 \end{aligned} \tag{2.6}$$

Substituting (2.5) in (2.6) yields the branch power equations:

$$\begin{aligned}
 P_{\text{branch}(i)} &= \sum_{k=1}^N G_{ik} V_{R(i)} V_{R(k)} + \sum_{k=1}^N G_{ik} V_{I(i)} V_{I(k)} \\
 &\quad + \sum_{k=1}^N B_{ik} V_{I(i)} V_{R(k)} - \sum_{k=1}^N B_{ik} V_{R(i)} V_{I(k)},
 \end{aligned} \tag{2.7}$$

and

$$\begin{aligned}
 Q_{\text{branch}(i)} &= \sum_{k=1}^N G_{ik} V_{I(i)} V_{R(k)} - \sum_{k=1}^N G_{ik} V_{R(i)} V_{I(k)} \\
 &\quad - \sum_{k=1}^N B_{ik} V_{R(i)} V_{R(k)} - \sum_{k=1}^N B_{ik} V_{I(i)} V_{I(k)}.
 \end{aligned} \tag{2.8}$$

## 2.3 Load Tap Changing (LTC) Transformer

A transformer that can provide a change in tap while it is energized is called a load tap changing (LTC) or tap changing under load (TCUL) transformer [32]. Figure 2.1a shows a one line diagram of the LTC transformer where “ $a$ ” is a real quantity representing the continuously changing tap setting.

The LTC transformer is modeled as an ideal machine. As illustrated in Figure 2.1b, all the complex power  $S_{\text{lrc}(k)} = P_{\text{lrc}(k)} + jQ_{\text{lrc}(k)}$  entering the primary terminals of the  $k^{\text{th}}$  LTC transformer is transferred to its secondary terminals. This



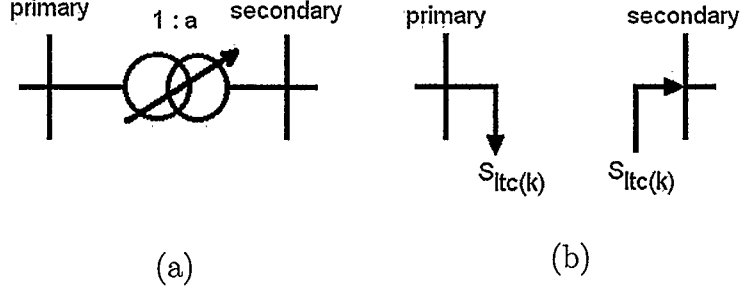


Figure 2.1: Illustration of the power transfer through a LTC transformer. (a) LTC transformer model. (b) The complex terminal power, denoted by  $S_{ltc(k)}$ , is transferred from the primary to the secondary side of the  $k^{\text{th}}$  LTC transformer [33].

approach for modeling the LTC transformer allows for easy incorporation into an optimization based program [33].

A continuous model of the LTC transformer can be given as [8, 23]:

$$\dot{a} = \frac{1}{T_t} (V_{ref} - V_t) \quad (2.9)$$

where  $T_t$  is the transformer time constant,  $V_{ref}$  is the reference voltage, and  $V_t$  is the controlled terminal voltage. The controlled voltage is defined as the magnitude of the voltage at the bus connected to the secondary side of the transformer and, in rectangular coordinates, it is given as:

$$\begin{aligned} V_t &= \sqrt{V_{R(secondary)}^2 + V_{I(secondary)}^2} \\ V_{R(secondary)} &= aV_{R(primary)} \\ V_{I(secondary)} &= aV_{I(primary)} \end{aligned} \quad (2.10)$$

where  $V_{R(primary)}$  and  $V_{I(primary)}$  are the real and imaginary components of the voltage at the bus connected to the primary side of the transformer; similarly,  $V_{R(secondary)}$

and  $V_{I(secondary)}$  are the real and imaginary components of the voltage at the bus connected to the secondary side of the transformer.

In an actual LTC transformer, the tap can be set only at discrete values: the continuous LTC model is not as accurate as the discrete model. However, this model is a valid approximation, particularly for mid to long term system stability analysis purposes where the time frame of interest is one to several minutes [8, 23].

## 2.4 Induction Machine

### 2.4.1 Introduction

Nicola Tesla developed the induction motor in 1887 based on a demonstration of the “Gramme dynamo”, a machine that could be operated either as a generator or as a motor [34]. An induction machine is a rotational electromechanical energy converter that is composed of a stationary member, referred to as the *stator*, and a rotating member, the *rotor*.

The main characteristics of a three-phase induction machine are:

- Three sinusoidally distributed Y- or  $\Delta$ -connected stator windings,
- Three sinusoidally distributed Y- or  $\Delta$ -connected rotor windings,
- An air gap to allow relative motion.

The induction machine has been mainly used as a motor since its invention. Induction motors are known as the workhorses of today’s industry [32].

In the following sections, the operating conditions of an induction motor are briefly explained. The conventional machine model is then developed using the

traditional method of reducing a symmetrical three phase machine to a two-axis (d-q) coil model on both the stator and the rotor, as described in [35].

#### 2.4.2 Slip and Operating Conditions

The stator windings are excited by applying a set of balanced three-phase voltages drawn from an external source of electrical energy. This causes currents to flow in the stator winding, which in turn produces a magnetic field. The produced magnetic field rotates at speed  $\omega_{sm}$  mechanical radians/seconds, referred to as the synchronous speed. This field induces voltage in the rotor windings, which produces sinusoidal currents in the rotor coils. The interaction between the rotor current with the stator field produces an electromechanical torque which spins the rotor [36]. If the developed torque is in the direction of the rotor movement, the machine is working as a motor.

A fundamental characteristic of an induction motor is the slip, which is defined as the relative speed between the rotor spinning at a steady speed  $\omega_{rm}$  and synchronously rotating stator field  $\omega_{sm}$  [35], that is

$$\text{slip} = \omega_{sm} - \omega_{rm}$$

For an induction motor, if there is no relative velocity between the stator and rotor fields (i.e. slip = 0), the induced rotor voltage and current will be zero, and consequently there would be no torque. Therefore, the rotor must settle at a sub-synchronous speed to develop a positive torque. In per unit system, the slip  $s$  is defined as [35]:

$$s \triangleq \frac{\omega_{sm} - \omega_{rm}}{\omega_{sm}} = \frac{\omega_e - \omega_r}{\omega_e} \quad (2.11)$$

where  $\omega_e = 2\pi f_e$  is defined as the angular speed of the excitation currents and the relation between electrical and mechanical angular speed, for a  $P$ -pole machine, can be given by [35]:

$$\begin{aligned}\omega_{sm} &= \frac{2}{P}\omega_e \\ \omega_{rm} &= \frac{2}{P}\omega_r\end{aligned}$$

### 2.4.3 Synchronously Rotating Reference Frame Transformation

The voltage equations that describe the behavior of ac machines contain time varying coefficients, due to the fact that some of the machine inductances are functions of the rotor displacement. Therefore, a change of variables (or transformation) is necessary to reduce the complexity of these voltage equations, by eliminating the time-dependent inductances [35, 37]. The reference frame transformation accomplishes such complexity reduction by replacing the stator and rotor “ $abc$ ” windings by fictitious “ $qd0$ ” windings, as discussed in this section.

The “ $abc$ ” quantities are transformed into “ $qd0$ ” quantities of a rotating reference frame with angular speed  $\omega_e$ , commonly known as synchronously rotating reference frame [35, 37]. In this reference frame, the “ $qd$ ” variables are constant in steady-state machine operation.

Figure 2.2 illustrates the relationship between the “ $abc$ ” stator and rotor quantities, and the corresponding “ $qd$ ” quantities. The “ $abc$ ” stator quantities may be thought of as varying along stationary axes  $as$ ,  $bs$ , and  $cs$ , each displaced by 120 electrical degrees. Similarly, the rotor “ $abc$ ” quantities vary along the  $ar$ ,  $br$ , and  $cr$  axes, each displaced by 120 electrical degrees and rotating at angular speed  $\omega_r$ . The

stator and rotor “ $abc$ ” quantities can be projected into the  $qd$  orthogonal axes; the  $qd$  reference frame rotates with angular speed  $\omega_e$ . The “0” variables are related only arithmetically to the “ $abc$ ” variables and are ignored in a balanced system, since these variables correspond to unbalanced currents and voltages.

The angle between the  $as$  axis and the  $q$  axis is denoted by  $\theta_e$ , and is expressed as:

$$\theta_e(t) = \int_0^t \omega_e(t)dt + \theta_e(0)$$

Analogously, the angle between  $as$  and  $ar$  axes is denoted by  $\theta_r$ , and is given by:

$$\theta_r(t) = \int_0^t \omega_r(t)dt + \theta_r(0)$$

The angles  $\theta_e(0)$  and  $\theta_r(0)$  are the initial values of the angles  $\theta_e$  and  $\theta_r$  respectively, at the beginning of time.

The transformation equation from “ $abc$ ” coordinates to “ $qd0$ ” coordinates can be written as [35]:

$$[\mathbf{f}_{qd0}] = [\mathbf{T}_{qd0}(\theta)][\mathbf{f}_{abc}] \quad (2.12)$$

where vector of variables,  $\mathbf{f}$ , may be voltages, currents, or flux linkages of the machine.

The “ $qd0$ ” transformation matrix is defined as:

$$[\mathbf{T}_{qd0}(\theta)] = \frac{2}{3} \begin{bmatrix} \cos \theta & \cos(\theta - \frac{2\pi}{3}) & \cos(\theta + \frac{2\pi}{3}) \\ \sin \theta & \sin(\theta - \frac{2\pi}{3}) & \sin(\theta + \frac{2\pi}{3}) \\ \frac{1}{2} & \frac{1}{2} & \frac{1}{2} \end{bmatrix} \quad (2.13)$$

The arbitrary angle of transformation  $\theta$  is substituted by  $\theta_e$  when changing the stator variables from “ $abc$ ” to the synchronously rotating “ $qd0$ ” reference frame. Likewise, the rotor quantities are transferred onto the same “ $qd$ ” reference frame (Figure 2.2) using  $\theta_e - \theta_r$  as the angle of transformation.

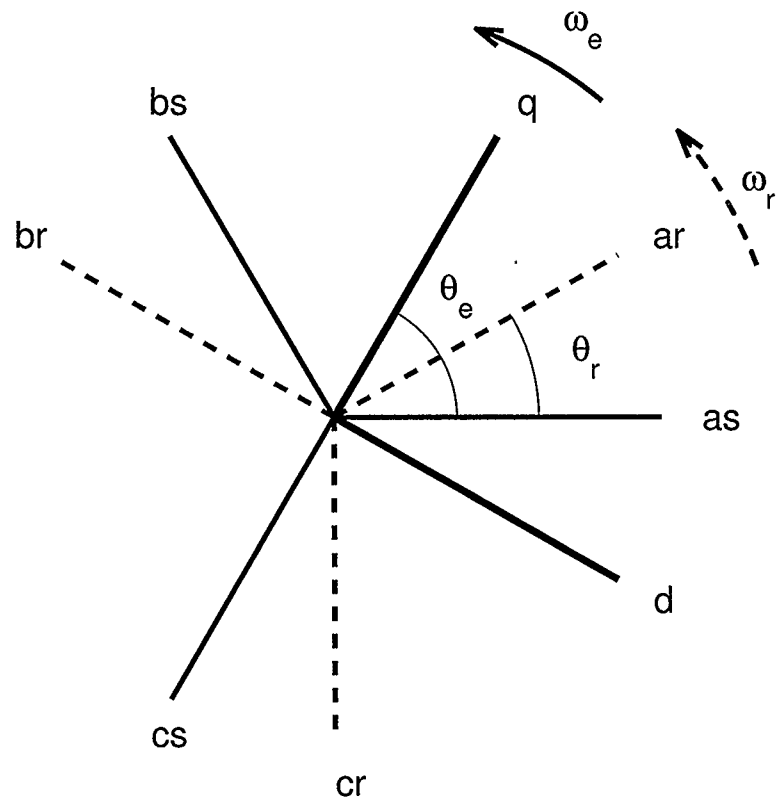


Figure 2.2: Relationship between stator and rotor  $abc$ -axes and synchronously rotating “ $qd0$ ” reference frame [35].

#### 2.4.4 Machine Model in the Synchronously Rotating “ $qd0$ ” Reference Frame

For analysis purposes, the actual physical machine is approximated by an ideal machine. The assumptions that are made to develop a mathematical model of an idealized machine are stated below [35]:

- Symmetrical air gap,
- Negligible hysteresis and eddy current losses,
- No saturation,
- Balanced voltage applied to the stator.

In the idealized machine, saturation or other non-linear effects are not modeled to keep the analysis simple [32].

The stator and rotor voltage equations in the “ $qd0$ ” synchronously rotating reference frame are stated below [35]:

$$\begin{aligned}
 v_{qs} &= r_s i_{qs} + \frac{1}{\omega_b} \dot{\psi}_{qs} + \frac{\omega_e}{\omega_b} \psi_{ds} \\
 v_{ds} &= r_s i_{ds} + \frac{1}{\omega_b} \dot{\psi}_{ds} - \frac{\omega_e}{\omega_b} \psi_{qs} \\
 v_{qr} &= r_r i_{qr} + \frac{1}{\omega_b} \dot{\psi}_{qr} + \frac{(\omega_e - \omega_r)}{\omega_b} \psi_{dr} \\
 v_{dr} &= r_r i_{dr} + \frac{1}{\omega_b} \dot{\psi}_{dr} - \frac{(\omega_e - \omega_r)}{\omega_b} \psi_{qr}
 \end{aligned} \tag{2.14}$$

where

- $v_{qs}, v_{ds}$  : the stator voltage along the “ $q$ ” and “ $d$ ” axes respectively,
- $v_{qr}, v_{dr}$  : the rotor voltage along the “ $q$ ” and “ $d$ ” axes respectively,

- $r_s$  : the stator winding resistance,
- $r_r$  : the rotor winding resistance,
- $i_{qs}, i_{ds}$  : the stator currents along the “ $q$ ” and “ $d$ ” axes,
- $i_{qr}, i_{dr}$  : the rotor currents along the “ $q$ ” and “ $d$ ” axes,
- $\omega_b$  : the base angular frequency, it is chosen to be equal to the synchronous speed  $\omega_e$
- $\psi_{qs}, \psi_{ds}$  : denotes the stator flux linkage per second along the “ $q$ ” and “ $d$ ” axes,
- $\psi_{qr}, \psi_{dr}$  : denotes the rotor flux linkage per second along the “ $q$ ” and “ $d$ ” axes,
- $\dot{\psi}_{qs}, \dot{\psi}_{ds}, \dot{\psi}_{qr}$ , and  $\dot{\psi}_{dr}$  : denotes the time derivative of the respective  $\psi_{qs}, \psi_{ds}, \psi_{qr}$ , and  $\psi_{dr}$  quantities.

The above set of equations, with the addition of the torque equation (to be presented in Section 2.4.5), form the dynamical model of the induction motor. In this model, the flux linkages per second  $\psi_{qs}, \psi_{ds}, \psi_{qr}$ , and  $\psi_{dr}$ , and the rotor angular speed  $\omega_r$  are the dynamical variables of the induction motor, and the stator terminal voltages  $v_{qs}, v_{ds}$  are the required inputs. The windings on the rotor are assumed to be short-circuited, therefore  $v_{qr} = 0$  and  $v_{dr} = 0$ . Equations corresponding to the “0” variables are omitted since the machine is assumed to be supplied by a balance external source.



The flux linkages per second are related to the stator and rotor currents by the following matrix equation:

$$\begin{bmatrix} \psi_{qs} \\ \psi_{ds} \\ \psi_{qr} \\ \psi_{dr} \end{bmatrix} = \begin{bmatrix} x_{ls} + x_m & 0 & x_m & 0 \\ 0 & x_{ls} + x_m & 0 & x_m \\ x_m & 0 & x_{lr} + x_m & 0 \\ 0 & x_m & 0 & x_{lr} + x_m \end{bmatrix} \begin{bmatrix} i_{qs} \\ i_{ds} \\ i_{qr} \\ i_{dr} \end{bmatrix} \quad (2.15)$$

where  $x_{ls}$  and  $x_{lr}$  are the stator and rotor windings leakage reactances respectively and  $x_m$  is the magnetizing reactance.

In order to incorporate the induction motor dynamical equations into the differential model of the system, it is necessary to isolate  $\dot{\psi}_{qs}$ ,  $\dot{\psi}_{ds}$ ,  $\dot{\psi}_{qr}$ , and  $\dot{\psi}_{dr}$  in (2.14). Furthermore, the stator and rotor current variables in (2.14) can be substituted by the flux linkages per second using (2.15), for simplification. Define the auxiliary quantities  $\psi_{mq}$ ,  $\psi_{md}$ , and  $x_M$ , as follows:

$$\begin{aligned} \psi_{mq} &= x_M \left( \frac{\psi_{qs}}{x_{ls}} + \frac{\psi_{qr}}{x_{lr}} \right) \\ \psi_{md} &= x_M \left( \frac{\psi_{ds}}{x_{ls}} + \frac{\psi_{dr}}{x_{lr}} \right) \\ \frac{1}{x_M} &= \frac{1}{x_m} + \frac{1}{x_{ls}} + \frac{1}{x_{lr}} \end{aligned} \quad (2.16)$$

Then, the stator and rotor currents can be computed from (2.15) and (2.16) using the following equations:

$$\begin{aligned} i_{qs} &= \frac{\psi_{qs} - \psi_{mq}}{x_{ls}} \\ i_{ds} &= \frac{\psi_{ds} - \psi_{md}}{x_{ls}} \\ i_{qr} &= \frac{\psi_{qr} - \psi_{mq}}{x_{lr}} \\ i_{dr} &= \frac{\psi_{dr} - \psi_{md}}{x_{lr}} \end{aligned} \quad (2.17)$$

Substituting (2.17) into (2.14), and isolating the time derivatives of the dynamical variables, yields:

$$\begin{aligned}
\dot{\psi}_{qs} &= \omega_b \left\{ v_{qs} - \frac{\omega_e}{\omega_b} \psi_{ds} + \frac{r_s}{x_{ls}} (\psi_{mq} - \psi_{qs}) \right\} \\
\dot{\psi}_{ds} &= \omega_b \left\{ v_{ds} + \frac{\omega_e}{\omega_b} \psi_{qs} + \frac{r_s}{x_{ls}} (\psi_{md} - \psi_{ds}) \right\} \\
\dot{\psi}_{qr} &= \omega_b \left\{ v_{qr} + \frac{\omega_r - \omega_e}{\omega_b} \psi_{dr} + \frac{r_r}{x_{lr}} (\psi_{mq} - \psi_{qr}) \right\} \\
\dot{\psi}_{dr} &= \omega_b \left\{ v_{dr} - \frac{\omega_r - \omega_e}{\omega_b} \psi_{qr} + \frac{r_r}{x_{lr}} (\psi_{md} - \psi_{dr}) \right\}
\end{aligned} \tag{2.18}$$

Let  $V_{R(i)}$  and  $V_{I(i)}$  be the real and imaginary components of the voltage at the  $i^{\text{th}}$  bus, where the machine is connected. The terminal voltage components  $V_{qs}$  and  $V_{ds}$  are related to  $V_{R(i)}$  and  $V_{I(i)}$  by the following equations:

$$v_{qs} = V_{R(i)} \tag{2.19}$$

$$v_{ds} = -V_{I(i)}$$

Moreover, the active and reactive power consumption of the machine can be computed as:

$$P_m = v_{qs} i_{qs} + v_{ds} i_{ds} \tag{2.20}$$

$$Q_m = v_{qs} i_{ds} - v_{ds} i_{qs}$$

Equations (2.19) and (2.20) represent the coupling between the induction motor equations and the power flow equations.

#### 2.4.5 Torque Equation

The final equation in the dynamical model of the induction motor is the swing equation, which represents Newton's second law for rotational movement: the net torque

applied to an object is directly proportional to the resulting angular acceleration and the moment of inertia of the object. Applying this concept, the motion of the rotor can be mathematically described as follows [35]:

$$\dot{\omega}_r = \frac{\omega_b}{2H}(T_{em} + T_{mech}) \quad (2.21)$$

where  $H$  is the inertia constant,  $T_{em}$  is the electromechanical torque produced by the motor, and  $T_{mech}$  is the mechanical load torque. The appearance of factor  $\omega_b$  in (2.21) is a consequence of the per unit normalization.

The produced electromechanical torque has the same direction as the rotor movement, thus  $T_{em} > 0$ . Conversely, the mechanical load torque opposes the rotor movement, in an induction motor, therefore  $T_{mech} < 0$

The electromechanical torque  $T_{em}$  is given by [35]:

$$T_{em} = (\psi_{ds}i_{qs} - \psi_{qs}i_{ds}) \quad (2.22)$$

In this thesis, the mechanical load torque  $T_{mech}$  is considered to be directly proportional to the normalized rotor speed, as proposed in [38], and is given in mathematical terms as:

$$T_{mech} = \lambda \frac{\omega_r}{\omega_b} \quad (2.23)$$

where the proportionality factor  $\lambda$  is a scalar that is known as the loading parameter (or loading factor) associated with the mechanical load of the induction motor. It is assumed in this work that all the mechanical loads present the same value of the loading parameter.

Equation (2.21) along with the set of equations given in (2.18) form the fifth order induction motor model used in this thesis.

## 2.5 Complete Model of the System

The system components modeled separately in the previous sections are now considered together to form a power system model represented by the following set of differential and algebraic equations (DAE):

$$\dot{\mathbf{x}} = \mathbf{F}(\mathbf{x}, \mathbf{y}; \lambda, \mathbf{p}), \quad (2.24)$$

$$0 = \mathbf{G}(\mathbf{x}, \mathbf{y}; \lambda, \mathbf{p}). \quad (2.25)$$

where

- $\mathbf{x} \in \mathbb{R}^D$  is the vector of system dynamic variables,  $D$  denotes the total number of the dynamic variables. These variables are also referred to as state variables, since they are used to describe the state of the system. Vector  $\mathbf{x}$  contains  $\psi_{qs}$ ,  $\psi_{ds}$ ,  $\psi_{qr}$ ,  $\psi_{dr}$ , and  $\omega_r$  for each induction machine, and  $a$  for each LTC transformer.
- $\dot{\mathbf{x}} \in \mathbb{R}^D$  represents the derivative of the state variables  $\mathbf{x}$  with respect to time,
- $\mathbf{y} \in \mathbb{R}^A$  is the vector of steady-state algebraic variables,  $A$  is the total number of algebraic variables. Vector  $\mathbf{y}$  contains  $v_{qs}$ ,  $v_{ds}$ ,  $P_m$ , and  $Q_m$  of each induction motor,  $P_{ltc}$  and  $Q_{ltc}$  for each LTC transformer,  $V_R$  and  $V_I$  at each network bus,  $Q_{gen}$  of each generator bus, and  $P_{gen}$  of the slack bus.
- $\lambda \in \mathbb{R}$  is the loading parameter, as shown in the previous section.
- $\mathbf{p} \in \mathbb{R}^{CP}$  is a set of controllable parameters,  $CP$  is the total number of controllable parameters in the system. In the proposed formulation, the controllable

parameters are the real component of the voltage at the slack bus, the magnitude of the voltage at each generator bus, the active power injected at the generator buses, and the reference voltage of the LTC transformers.

The set of differential equations (2.24) represents the induction motor model of (2.18) and (2.21), and the LTC transformer dynamics in (2.9). The set of algebraic equations (2.25) represents the power flow equations in (2.1) and (2.2), and the algebraic equations of induction motors and LTC transformers in (2.19), (2.20), and (2.10).

## 2.6 Summary

In this chapter, the following concepts are reviewed:

- Power flow equations in rectangular coordinates;
- A continuous model of LTC transformers;
- A dynamical 5<sup>th</sup> order model of induction motors, in the synchronously rotating reference frame.

These elements are incorporated into a single power network differential-algebraic model. It will be shown in the next chapter that such model is adequate for system stability analysis and the study of Hopf bifurcations.

## Chapter 3

# Power System Instability and Bifurcations

### 3.1 Introduction

Today's power networks operate close to their control and operational limits, due to the ever increasing demand for electrical energy, and the economical and environmental restrictions on power systems expansion [39]. Such highly stressed systems can exhibit scenarios of instability [40]. Consequently, system stability analysis is of major interest in the planning and operating present day power system networks.

Generally, if one or more system parameters vary continually in a particular direction, a critical point may be reached where a qualitative change occurs in the system state. For instance, the system might change from stable equilibrium to unstable equilibrium or a limit cycle oscillation. This phenomenon is known as *bifurcation*. Saddle-node and Hopf bifurcations have been recognized as the main reasons behind system instability in power systems [7, 5]. The occurrence of saddle-node and Hopf bifurcations is characterized by a change in the small-disturbance stability properties of the power system.

Small-disturbance system stability analysis of a power system is the study of the system's response to small perturbations [9]. In this limited range of operation, the nonlinear system of differential and algebraic (D-A) equations can be linearized around an equilibrium point. The eigenvalues of the linearized model are then used to determine the stability of the linear system.

This chapter reviews the theory of small-disturbance stability analysis of power systems, followed by an introduction to bifurcation analysis, with an emphasis on saddle-node and Hopf bifurcations. Methods to predict and detect bifurcations are subsequently presented. Finally, application of optimization theory for system stability analysis is introduced.

### 3.2 Small-disturbance Power System Stability Analysis

Small-disturbance system stability is defined as the system's ability to return to the equilibrium point under investigation when subjected to small perturbations [9]. The small-disturbance system stability analysis examines the eigenvalues of the linearized model to determine the system stability condition.

Consider the system model presented in Section 2.5:

$$\dot{\mathbf{x}} = \mathbf{F}(\mathbf{x}, \mathbf{y}; \lambda, \mathbf{p}), \quad (3.1)$$

$$0 = \mathbf{G}(\mathbf{x}, \mathbf{y}; \lambda, \mathbf{p}). \quad (3.2)$$

where  $\mathbf{F}(\cdot)$  and  $\mathbf{G}(\cdot)$  represent the dynamic and algebraic equations,  $\mathbf{x}$  and  $\mathbf{y}$  are the dynamic and algebraic variables,  $\lambda$  is the loading parameter and  $\mathbf{p}$  is the vector of controllable parameters of the system.

The power system model given by (3.1) and (3.2) will be linearized around an equilibrium point (i.e  $\dot{\mathbf{x}} = 0$ ). Let the vector  $\mathbf{x}_0$  and  $\mathbf{y}_0$  be the solution of the system at the equilibrium point for a fixed value of the loading parameter  $\lambda_0$  and fixed vector

of controllable parameters  $\mathbf{p}_0$ , that is:

$$\mathbf{F}(\mathbf{x}_0, \mathbf{y}_0; \lambda_0, \mathbf{p}_0) = \mathbf{0}, \quad (3.3)$$

$$\mathbf{G}(\mathbf{x}_0, \mathbf{y}_0; \lambda_0, \mathbf{p}_0) = \mathbf{0}. \quad (3.4)$$

The system may then be subjected to a small-disturbance, obtaining:

$$\mathbf{x} = \mathbf{x}_0 + \Delta\mathbf{x}, \quad (3.5)$$

$$\mathbf{y} = \mathbf{y}_0 + \Delta\mathbf{y}, \quad (3.6)$$

where  $\Delta\mathbf{x}$  and  $\Delta\mathbf{y}$  denote perturbations in the dynamic and algebraic variables of the system respectively. Note that taking the time derivative of both sides of (3.5) yields:  $\dot{\mathbf{x}} = \dot{\mathbf{x}}_0 + \Delta\dot{\mathbf{x}} = \Delta\dot{\mathbf{x}}$ , since  $\mathbf{x}_0$  is a constant value. The above expressions are introduced in the differential-algebraic system of equations (3.1) and (3.2), and their Taylor series expansion is written as:

$$\begin{aligned} \dot{\mathbf{x}} &= \Delta\dot{\mathbf{x}} = \mathbf{F}[(\mathbf{x}_0 + \Delta\mathbf{x}), (\mathbf{y}_0 + \Delta\mathbf{y}); \lambda_0, \mathbf{p}_0] \\ &= \mathbf{F}(\mathbf{x}_0, \mathbf{y}_0, \lambda_0, \mathbf{p}_0) + \mathbf{J}_1\Delta\mathbf{x} + \mathbf{J}_2\Delta\mathbf{y} + \text{H.O.T} \end{aligned} \quad (3.7)$$

$$\begin{aligned} \mathbf{0} &= \mathbf{G}[(\mathbf{x}_0 + \Delta\mathbf{x}), (\mathbf{y}_0 + \Delta\mathbf{y}); \lambda_0, \mathbf{p}_0] \\ &= \mathbf{G}(\mathbf{x}_0, \mathbf{y}_0, \lambda_0, \mathbf{p}_0) + \mathbf{J}_3\Delta\mathbf{x} + \mathbf{J}_4\Delta\mathbf{y} + \text{H.O.T} \end{aligned} \quad (3.8)$$

where H.O.T stands for the Higher Order terms, and the matrices  $\mathbf{J}_1$ ,  $\mathbf{J}_2$ ,  $\mathbf{J}_3$ , and  $\mathbf{J}_4$



are presented below:

$$\begin{aligned}
 \mathbf{J}_1 &= \begin{bmatrix} \frac{\partial f_1(\cdot)}{\partial x_1} & \cdots & \frac{\partial f_1(\cdot)}{\partial x_D} \\ \frac{\partial f_2(\cdot)}{\partial x_1} & \cdots & \frac{\partial f_2(\cdot)}{\partial x_D} \\ \vdots & \ddots & \vdots \\ \frac{\partial f_D(\cdot)}{\partial x_1} & \cdots & \frac{\partial f_D(\cdot)}{\partial x_D} \end{bmatrix} & \mathbf{J}_2 &= \begin{bmatrix} \frac{\partial f_1(\cdot)}{\partial y_1} & \cdots & \frac{\partial f_1(\cdot)}{\partial y_A} \\ \frac{\partial f_2(\cdot)}{\partial y_1} & \cdots & \frac{\partial f_2(\cdot)}{\partial y_A} \\ \vdots & \ddots & \vdots \\ \frac{\partial f_D(\cdot)}{\partial y_1} & \cdots & \frac{\partial f_D(\cdot)}{\partial y_A} \end{bmatrix} \\
 \mathbf{J}_3 &= \begin{bmatrix} \frac{\partial g_1(\cdot)}{\partial x_1} & \cdots & \frac{\partial g_1(\cdot)}{\partial x_D} \\ \frac{\partial g_2(\cdot)}{\partial x_1} & \cdots & \frac{\partial g_2(\cdot)}{\partial x_D} \\ \vdots & \ddots & \vdots \\ \frac{\partial g_A(\cdot)}{\partial x_1} & \cdots & \frac{\partial g_A(\cdot)}{\partial x_D} \end{bmatrix} & \mathbf{J}_4 &= \begin{bmatrix} \frac{\partial g_1(\cdot)}{\partial y_1} & \cdots & \frac{\partial g_1(\cdot)}{\partial y_A} \\ \frac{\partial g_2(\cdot)}{\partial y_1} & \cdots & \frac{\partial g_2(\cdot)}{\partial y_A} \\ \vdots & \ddots & \vdots \\ \frac{\partial g_A(\cdot)}{\partial y_1} & \cdots & \frac{\partial g_A(\cdot)}{\partial y_A} \end{bmatrix}
 \end{aligned} \tag{3.9}$$

The total number of dynamic variables is denoted by  $D$  and the total number of algebraic variables in the system is  $A$ . The partial derivatives in the preceding matrices are calculated at the equilibrium point  $(\mathbf{x}_0, \mathbf{y}_0, \lambda_0, \mathbf{p}_0)$ .

Since  $\mathbf{F}(\mathbf{x}_0, \mathbf{y}_0, \lambda_0, \mathbf{p}_0) = \mathbf{0}$  and  $\mathbf{G}(\mathbf{x}_0, \mathbf{y}_0, \lambda_0, \mathbf{p}_0) = \mathbf{0}$ , these components can be eliminated from (3.7) and (3.8). Furthermore, the higher order terms can be ignored given that the perturbation is sufficiently small. The linearized equations can then be written as the following:

$$\Delta \dot{\mathbf{x}} = \mathbf{J}_1 \Delta \mathbf{x} + \mathbf{J}_2 \Delta \mathbf{y} \tag{3.10}$$

$$\mathbf{0} = \mathbf{J}_3 \Delta \mathbf{x} + \mathbf{J}_4 \Delta \mathbf{y} \tag{3.11}$$

The matrices  $\mathbf{J}_1 \in \mathbb{R}^{D \times D}$ ,  $\mathbf{J}_2 \in \mathbb{R}^{D \times A}$ ,  $\mathbf{J}_3 \in \mathbb{R}^{A \times D}$ , and  $\mathbf{J}_4 \in \mathbb{R}^{A \times A}$  form the Jacobian matrix of the system ( $\mathbf{J} \in \mathbb{R}^{(D+A) \times (D+A)}$ ) as below:

$$\mathbf{J} = \left[ \begin{array}{c|c} \mathbf{J}_1 & \mathbf{J}_2 \\ \hline \mathbf{J}_3 & \mathbf{J}_4 \end{array} \right] \tag{3.12}$$

Assuming  $\mathbf{J}_4$  is a nonsingular matrix, then (3.11) can be solved in terms of  $\Delta \mathbf{y}$ , yielding:

$$\Delta \mathbf{y} = -\mathbf{J}_4^{-1} \mathbf{J}_3 \Delta \mathbf{x} \quad (3.13)$$

Substituting (3.13) into (3.10) results into the following:

$$\Delta \dot{\mathbf{x}} = \underbrace{[\mathbf{J}_1 - \mathbf{J}_2 \mathbf{J}_4^{-1} \mathbf{J}_3]}_{\mathbf{J}_{\text{reduced}}} \Delta \mathbf{x} \quad (3.14)$$

where the matrix  $\mathbf{J}_{\text{reduced}} \in \mathbb{R}^{D \times D}$  is called the reduced Jacobian or the state matrix of the system.

It is shown in Appendix A that the time solution of the above problem can be given by [32]:

$$\Delta \mathbf{x}(t) = \sum_{i=1}^D \Phi_i \Psi_i \Delta \mathbf{x}(0) e^{\eta_i t} \quad (3.15)$$

where

$\Phi_i \in \mathbb{C}^{D \times 1}$  is the  $i^{\text{th}}$  right eigenvector of  $\mathbf{J}_{\text{reduced}}$ ,

$\Psi_i \in \mathbb{C}^{1 \times D}$  is the  $i^{\text{th}}$  left eigenvector of  $\mathbf{J}_{\text{reduced}}$ ,

$\Delta \mathbf{x}(0) \in \mathbb{R}^D$  is the initial value of  $\Delta \mathbf{x}$ ,

$\eta_i$  is the  $i^{\text{th}}$  eigenvalue of  $\mathbf{J}_{\text{reduced}}$ .

The eigenvalues  $\eta_i$  are either real, or form complex conjugate pairs, since  $\mathbf{J}_{\text{reduced}}$  is real [41]. The eigenvalues of the system correspond to different modes, as follows [32]:

- a) A negative real eigenvalue represents a non-oscillatory exponentially decaying mode.

- b) A positive real eigenvalue represents a non-oscillatory mode with exponential growth.
- c) A complex conjugate pair of eigenvalues represents an oscillatory mode. If the real part of the eigenvalue is negative, the amplitude of the oscillation will decay exponentially; otherwise, there will be an exponentially increasing amplitude in the oscillation.

If all the eigenvalues of (3.15) have negative real parts, the system is stable. Otherwise, there will be a mode (oscillatory or non-oscillatory) of the system with exponential growth. The particular case where a real eigenvalue or a complex conjugate pair have zero real part will be discussed in Sections 3.3.1 and 3.3.2.

### 3.3 Bifurcation Theory

Bifurcation theory describes the possible ways in which a system can become unstable as a system parameter varies slowly. This theory is applied in power systems small-disturbance system stability analysis to identify the operating points where significant changes occur in the system state, as the loading parameter is changed. These points are referred to as bifurcation points [8]. The distance to a bifurcation is defined, in this thesis, as the difference between the loading parameter values at the bifurcation point and at the normal operating point.

Two types of bifurcation are often associated with the instability and/or collapse in power systems [7, 5]: saddle-node bifurcation, and Hopf bifurcation.

### 3.3.1 Saddle-Node Bifurcations (SNB)

The concept of saddle-node bifurcation can be better explained using a bifurcation diagram, as shown in Figure 3.1. The bifurcation diagram is a graphical display of the steady-state solutions of the system in the  $(\mathbf{x}, \mathbf{y}, \lambda)$  space, and it generally consists of lines in this multidimensional space [6]. As it is shown in Figure 3.1, where  $z$  is typically a load bus voltage magnitude in power systems, for  $\lambda < \lambda_{\text{SNB}}$  there are two solutions to the system equations, at  $\lambda = \lambda_{\text{SNB}}$  there is only one solution and beyond this value of  $\lambda$  there is no equilibrium solution for the system. In this case,  $\lambda = \lambda_{\text{SNB}}$  is the maximum system loadability. The saddle-node bifurcation (SNB) is defined as a point where two branches of equilibrium points meet and there is no equilibrium solution beyond the point of intersection [6] .

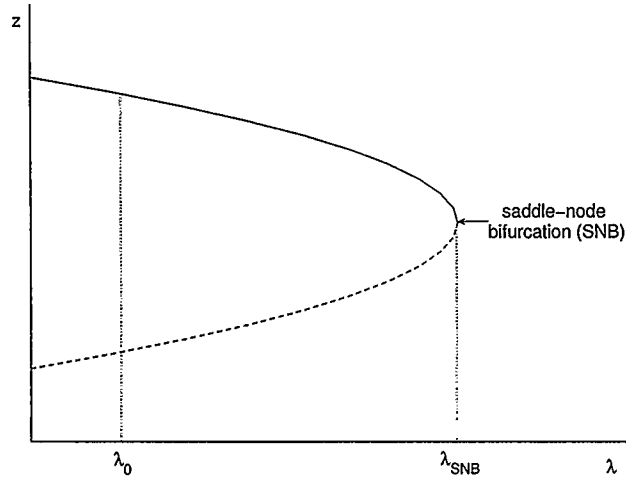


Figure 3.1: Example of a bifurcation diagram showing saddle-node bifurcation, where  $z$  is typically a load bus voltage magnitude in power systems

At the point of SNB the following conditions are valid [6]:

- 1) Saddle-node bifurcation occurs at an equilibrium point, i.e.  $\mathbf{F}(\mathbf{x}^*, \mathbf{y}^*; \lambda_{\text{SNB}}, \mathbf{p}^*) =$

$$\mathbf{0} \text{ and } \mathbf{G}(\mathbf{x}^*, \mathbf{y}^*; \lambda_{\text{SNB}}, \mathbf{p}^*) = \mathbf{0},$$

- 2) The full Jacobian matrix of the system has a simple and unique zero eigenvalue, implying a singular Jacobian matrix,
- 3) At the saddle-node two branches of equilibria intersect and both disappear beyond the SNB point.

Saddle-node bifurcations can be associated with the voltage collapse in power systems, and therefore have been thoroughly studied in literature, for example, [24, 42, 43, 44, 45].

### 3.3.2 Hopf Bifurcations

Hopf Bifurcation (HB) (or oscillatory bifurcation) is defined as a bifurcation that connects equilibria with periodic oscillation [6]. These types of oscillatory problems are encountered in power networks [46].

The basic theory behind the Hopf bifurcation can be explained using the DAE model of a power system given by (3.1) and (3.2). As the loading parameter ( $\lambda$ ) varies slowly, the equilibrium points ( $\mathbf{x}_0, \mathbf{y}_0$ ) change and consequently the eigenvalues of the reduced Jacobian matrix of the system move in the complex plane. The point  $(\mathbf{x}^*, \mathbf{y}^*, \lambda_{\text{HB}}, \mathbf{p}^*)$  where a pair of complex conjugate eigenvalues reaches the imaginary axis is a Hopf bifurcation point if the following conditions are satisfied [6]:

- 1)  $\mathbf{F}(\mathbf{x}^*, \mathbf{y}^*; \lambda_{\text{HB}}, \mathbf{p}^*) = \mathbf{0}$  and  $\mathbf{G}(\mathbf{x}^*, \mathbf{y}^*; \lambda_{\text{HB}}, \mathbf{p}^*) = \mathbf{0}$ ,
- 2) The reduced Jacobian matrix evaluated at the solution of above equations should have a simple pair of purely imaginary eigenvalues (known as critical

eigenvalues), that is  $\eta = \pm j\beta$ , and no other eigenvalues with zero real parts,

- 3) The rate of change of the real part of the critical eigenvalues with respect to  $\lambda$  should be nonzero, that is  $\frac{\partial \text{Re}(\eta)}{\partial \lambda} \neq 0$ . In other words, the system is changing its stability characteristic.

In this event, the system is experiencing a Hopf bifurcation and the initial period of the limit cycle ( $T_0$ ) can be computed as [6]:

$$T_0 = \frac{2\pi}{\beta} \quad (3.16)$$

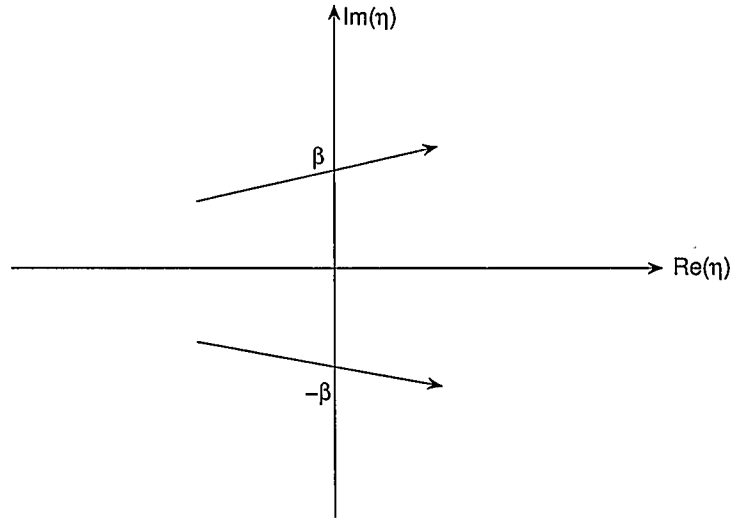


Figure 3.2: A complex conjugate pair of purely imaginary eigenvalues crossing the imaginary axis

The above mentioned conditions imply that Hopf bifurcation corresponds to a system equilibrium state with a pair of purely imaginary eigenvalues crossing the imaginary axis as a system parameter (i.e.  $\lambda$ ) varies, yielding oscillations in the system. The pair of complex conjugate eigenvalues crossing the imaginary axis is depicted in Figure 3.2.

### 3.4 Methods to Detect Bifurcations

The occurrence of bifurcation is a limiting factor in power systems operation. Therefore, the ability to predict the distance to the bifurcation point is a valuable asset to the system operators. In this section, two different indices of proximity to bifurcation are presented, followed by a discussion on the continuation method, which provides a measure of the distance to the bifurcation point.

#### 3.4.1 Singular Value and Eigenvalue indices

Eigenvalues and singular values are used in power system literature to determine proximity to system bifurcations [42, 19].

##### Eigenvalue Index (EVI)

All the eigenvalues of a system at stable equilibrium have negative real part. As the system's loading parameter is increased, a bifurcation point can be reached. In this case, the system will exhibit a single zero eigenvalue (saddle-node bifurcation) or a single pair of complex conjugate eigenvalues with zero real part (Hopf bifurcation).

Based on the aforementioned observation, the Eigenvalue Index (EVI) is defined as [6]:

$$EVI = |\alpha| \quad (3.17)$$

where  $\alpha$  is the real part of eigenvalue with the largest real part. Such an eigenvalue is referred to as the critical eigenvalue of the system.

Observe that the EVI is zero when a bifurcation point is reached. The EVI is an indirect measure of the distance to bifurcation, when the system is operating close to the bifurcation point. This index is rather insensitive to the increase of

the loading parameter unless the system is operating in the vicinity of a bifurcation point, as discussed in [5]. Therefore, the eigenvalue index cannot be used to predict the bifurcation well in advance [19].

### Singular value index

The eigenvalue problem for the critical complex eigenvalue of the system can be written as:

$$\mathbf{J}_{\text{reduced}} [\mathbf{v}_R + j\mathbf{v}_I] = (\alpha + j\beta) [\mathbf{v}_R + j\mathbf{v}_I] \quad (3.18)$$

where matrix  $\mathbf{J}_{\text{reduced}}$  is the reduced Jacobian matrix of the system;  $\alpha$  and  $\beta$  are the real and imaginary components of the critical eigenvalue  $\eta$  (note that, if  $\beta > 0$ , the conjugate  $\eta^*$  is also a critical eigenvalue of  $\mathbf{J}_{\text{reduced}}$ ); the vectors  $\mathbf{v}_R$  and  $\mathbf{v}_I$  are the real and imaginary component of the eigenvector  $\mathbf{v}$  associated with the eigenvalue  $\eta$ . After separating the real and imaginary components (3.18) can be rewritten in matrix form as:

$$\left( \underbrace{\begin{bmatrix} \mathbf{J}_{\text{reduced}} & +\beta\mathbf{I}_n \\ -\beta\mathbf{I}_n & \mathbf{J}_{\text{reduced}} \end{bmatrix}}_{\mathbf{A}_m} - \alpha\mathbf{I}_{2n} \right) \begin{bmatrix} \mathbf{v}_R \\ \mathbf{v}_I \end{bmatrix} = \mathbf{0} \quad (3.19)$$

Matrices  $\mathbf{I}_n \in \mathbb{R}^{D \times D}$  and  $\mathbf{I}_{2n} \in \mathbb{R}^{2D \times 2D}$  are the identity matrices of proper size,  $D$  is the number of state variables.

When  $\alpha = 0$  the modified reduced Jacobian matrix  $\mathbf{A}_m$  becomes singular, since the eigenvectors are nonzero. The minimum singular value  $\sigma_{\min}$  of this modified matrix is used as an index to detect Hopf bifurcation, as proposed in [47], and stated in mathematical terms below:

$$\text{HBI}_1(\mathbf{J}_{\text{reduced}}, \beta) = \sigma_{\min}(\mathbf{A}_m) \quad (3.20)$$



This index is considered to be computationally expensive as it requires the calculation of the matrix  $\mathbf{J}_{\text{reduced}}$ , which involves matrix inversion.

### 3.4.2 Continuation Method

The loading margin of a power system, for a particular operating point, is the amount of additional load in a specific pattern of load increase that would bring the system to a bifurcation point. The loading margin corresponds to the maximum system loadability. It is crucial for system analysis to be able to determine the amount of load increase that would cause instability.

The continuation method permits the computation of the maximum system loadability, by computing successive equilibrium points of the system as the loading parameter is slowly varied. A continuation method can be considered mainly as a two step approach [8]: the predictor step and the corrector step. The predictor step starts with a known solution and uses a tangent predictor to estimate the next solution. This estimate is then corrected at the corrector step by computing a solution on the bifurcation diagram perpendicular to the predictor solution, as depicted in Figure 3.3.

The algorithm starts with a known equilibrium point  $(\mathbf{x}_0, \mathbf{y}_0, \lambda_0, \mathbf{p}_0)$ , and the controllable parameters  $\mathbf{p}_0$  are fixed. Let  $(\mathbf{x}_i, \mathbf{y}_i, \lambda_i, \mathbf{p}_0)$  be the equilibrium solution computed at the  $i^{\text{th}}$  step. The continuation method proceeds as follows:

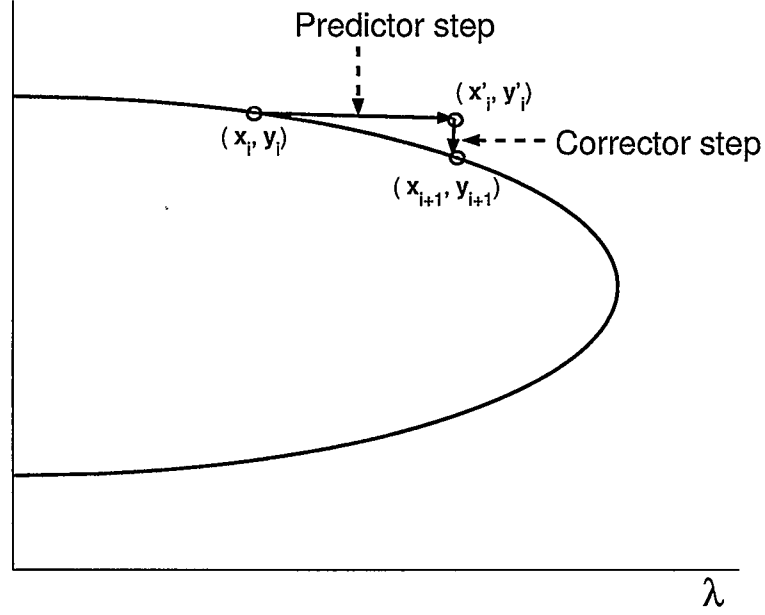


Figure 3.3: Bifurcation diagram obtained by continuation method

#### Predictor Step:

The equation that defines the equilibrium point  $(\mathbf{x}_i, \mathbf{y}_i, \lambda_i, \mathbf{p}_0)$  is given by:

$$\mathbf{F}(\mathbf{x}_i, \mathbf{y}_i, \lambda_i, \mathbf{p}_0) = \mathbf{0} \quad (3.21)$$

$$\mathbf{G}(\mathbf{x}_i, \mathbf{y}_i, \lambda_i, \mathbf{p}_0) = \mathbf{0} \quad (3.22)$$

Applying the Chain Rule to take the total derivative of both functions with respect to the loading parameter  $\lambda$ , yields:

$$\mathbf{J}_1 \frac{d\mathbf{x}}{d\lambda} + \mathbf{J}_2 \frac{d\mathbf{y}}{d\lambda} + \frac{\partial \mathbf{F}(\cdot)}{\partial \lambda} \frac{d\lambda}{d\lambda} = \mathbf{0} \quad (3.23)$$

$$\mathbf{J}_3 \frac{d\mathbf{x}}{d\lambda} + \mathbf{J}_4 \frac{d\mathbf{y}}{d\lambda} + \frac{\partial \mathbf{G}(\cdot)}{\partial \lambda} \frac{d\lambda}{d\lambda} = \mathbf{0} \quad (3.24)$$

where  $\mathbf{J}_1$ ,  $\mathbf{J}_2$ ,  $\mathbf{J}_3$ , and  $\mathbf{J}_4$  are defined in (3.9).

Equations (3.23) and (3.24) can be simplified and rearranged into matrix form

as given below:

$$\underbrace{\begin{bmatrix} \mathbf{J}_1 & \mathbf{J}_2 \\ \mathbf{J}_3 & \mathbf{J}_4 \end{bmatrix}}_{\mathbf{J}} \underbrace{\begin{bmatrix} \frac{dx}{d\lambda} \\ \frac{dy}{d\lambda} \end{bmatrix}}_{\mathbf{z}} = - \underbrace{\begin{bmatrix} \frac{\partial \mathbf{F}(\cdot)}{\partial \lambda} \\ \frac{\partial \mathbf{G}(\cdot)}{\partial \lambda} \end{bmatrix}}_{\mathbf{b}} \quad (3.25)$$

where  $\mathbf{J}_1, \mathbf{J}_2, \mathbf{J}_3, \mathbf{J}_4, \frac{\partial \mathbf{F}(\cdot)}{\partial \lambda}$ , and  $\frac{\partial \mathbf{G}(\cdot)}{\partial \lambda}$  are evaluated at the current equilibrium solution  $(\mathbf{x}_i, \mathbf{y}_i, \lambda_i, \mathbf{p}_0)$ . This linear system is solved in order to obtain  $\frac{dx}{d\lambda}$  and  $\frac{dy}{d\lambda}$ . The change of system parameter can be defined as [5]:

$$\Delta\lambda \triangleq \frac{k}{\|\mathbf{z}\|_\infty} \quad (3.26)$$

while  $0 < k \leq 1$  controls the size of the predictor step. Since the predictor vector is tangent to the bifurcation diagram, the variation in the state and algebraic variables is defined by [5]:

$$\Delta\mathbf{x} \triangleq \frac{d\mathbf{x}}{d\lambda} \Delta\lambda \quad (3.27)$$

$$\Delta\mathbf{y} \triangleq \frac{d\mathbf{y}}{d\lambda} \Delta\lambda \quad (3.28)$$

A predicted solution  $(\mathbf{x}'_i, \mathbf{y}'_i, \lambda'_i, \mathbf{p}_0)$  for solving the system equations at the new load setting is obtained as:

$$\mathbf{x}'_i = \mathbf{x}_i + \Delta\mathbf{x} \quad (3.29)$$

$$\mathbf{y}'_i = \mathbf{y}_i + \Delta\mathbf{y} \quad (3.30)$$

$$\lambda'_i = \lambda_i + \Delta\lambda \quad (3.31)$$

#### Corrector Step:

The results obtained from the predictor step are used to compute a new equilibrium point  $(\mathbf{x}_{i+1}, \mathbf{y}_{i+1}, \lambda_{i+1}, \mathbf{p}_0)$  on the bifurcation diagram by solving the following

set of equations [5]:

$$\mathbf{F}(\mathbf{x}_{i+1}, \mathbf{y}_{i+1}, \lambda_{i+1}, \mathbf{p}_0) = \mathbf{0} \quad (3.32)$$

$$\mathbf{G}(\mathbf{x}_{i+1}, \mathbf{y}_{i+1}, \lambda_{i+1}, \mathbf{p}_0) = \mathbf{0} \quad (3.33)$$

$$\begin{bmatrix} \Delta \mathbf{x}^T & \Delta \mathbf{y}^T & \Delta \lambda \end{bmatrix} \begin{bmatrix} \mathbf{x}_{i+1} - \mathbf{x}'_i \\ \mathbf{y}_{i+1} - \mathbf{y}'_i \\ \lambda_{i+1} - \lambda'_i \end{bmatrix} = \mathbf{0} \quad (3.34)$$

The above nonlinear system of equations is solved using a Newton-Raphson method, with  $(\mathbf{x}'_i, \mathbf{y}'_i, \lambda'_i, \mathbf{p}_0)$  as the initial solution. The first and second equations in (3.32) corresponds to the steady-state system equations. The third equation represents the perpendicularity between the predictor and the corrector vectors.

### 3.5 Optimal Power Flow (OPF)

Optimal power flow (OPF) problem is formulated to find the values of the system variables and controllable parameters that minimize some cost function of the system while enforcing a variety of equality and/or inequality constraints [4]. The general concept of a classical OPF problem can be explained as follows:

- objective function
  - Minimize (or maximize) an objective function of the power system. Examples of objective functions that have been proposed in the literature include:
    - \* active power losses
    - \* loadability limit of the system

- subject to
  - Active and reactive power balance in the system. These equations are expressed as equality constraints in the problem.
  - The operating and/or physical limits of the system, such as limits on bus voltage or active and reactive power generation. The limits are expressed as inequality constraints.

In mathematical terms a classical optimal power flow problem with the objective of maximizing the system loading margin can be written as:

**objective function:**

$$\max \lambda_c$$

**subject to:**

$$G(\mathbf{y}; \lambda_c, \mathbf{p}) = 0 \quad (3.35)$$

$$\underline{\mathbf{p}} \leq \mathbf{p} \leq \bar{\mathbf{p}} \quad (3.36)$$

$$\underline{\mathbf{h}} \leq \mathbf{h}(\mathbf{y}) \leq \bar{\mathbf{h}} \quad (3.37)$$

where:

$\lambda_c$ : critical loading parameter of the system,

$\underline{\mathbf{p}}, \bar{\mathbf{p}}$ : lower and upper bounds for the controllable parameters,

$\underline{\mathbf{h}}, \bar{\mathbf{h}}$ : lower and upper bounds for the voltage at each bus,

$\mathbf{h} : \mathbb{R}^A \rightarrow \mathbb{R}^N$ : represents the voltage magnitude at each bus.

Such a formulation does not consider the limitation in the loading margin that is introduced by the presence of Hopf bifurcations. In Chapter 4 several strategies for the inclusion of Hopf bifurcation into the optimization procedure will be discussed.

In general, OPF is a nonlinear, nonconvex optimization problem [48]. Optimization methods that are suitable to solve the OPF problem include sequential quadratic programming and nonlinear interior point methods [49, 50, 48].

### 3.6 Summary

The goal of small-disturbance system stability analysis is to investigate the stability of a power system at equilibrium, as the system is subjected to a small perturbation. In this analysis, the system model is linearized around the equilibrium point, and the eigenvalues of the reduced Jacobian matrix are used to determine the stability characteristic of the system.

A continuous increase in the loading parameter  $\lambda$  of the system results in the movement of the equilibrium point in the  $\mathbf{x}, \mathbf{y}, \lambda$  space. The system may then reach a point where any further increase in the loading parameter will cause a change in the stability characteristic of the equilibrium point. This limiting point is called a bifurcation point.

Bifurcation points can be classified into different types, according to the movement of the system eigenvalues. The system experiences a Hopf bifurcation, if a pair of complex conjugate eigenvalues of the linearized system crosses the imaginary axis in the complex plane, from the left to the right, yielding system oscillations. Saddle-node bifurcation occurs if an eigenvalue of the system matrix becomes purely

real and equals to zero with all other eigenvalues having nonzero real parts.

Several methods to detect saddle-node and Hopf bifurcations have been discussed in this chapter. The optimal power flow problem is formulated and discussed as a means to obtain the maximum system loadability. It is noticed that the classical formulation of the OPF problem does not include any constraints with respect to the occurrence of any type of bifurcations in the system.

# Chapter 4

## Optimal Power Flow with Hopf Bifurcation Constraints

### 4.1 Introduction

A major aspect of power systems operation is to increase the system security margin by readjusting the network control configuration. As presented in Section 3.5, the classical optimal power flow (OPF) problem does not incorporate the dynamics of the system, and consequently is not an appropriate tool to maximize the system loadability with respect to the occurrence of Hopf bifurcations.

The study of oscillatory problems (such as Hopf bifurcations) in a power network requires the consideration of the dynamics of the system [11, 13, 51]. In this regard, the algebraic and differential equations of voltage dependent loads (induction motors) and continuous control devices (LTC transformers) are incorporated into the classical optimization problem, since the interaction of LTC transformer with the load significantly affects the development of the Hopf bifurcation [52].

The goal of this research is to improve the small-disturbance stability margin of a power system, through optimal setting of the system's controllable parameters. The system differential-algebraic equations (DAE) are modeled to account for the possibility of occurrence of Hopf bifurcation. In order to achieve this goal, two approaches are proposed and investigated:



1. Maximize the system loadability with respect to the Hopf Bifurcation (HB) point: the mathematical conditions that define the HB point are explicitly modeled. The optimization goal is to compute the maximum system loadability (MSL) related to Hopf bifurcations. Three optimization problems are defined within this category: Generalized Eigenvalue Based Hopf Bifurcation Constrained OPF (GEHB-OPF), Critical Eigenvalue Based Hopf Bifurcation Constrained OPF (CEHB-OPF), and Stability Constrained OPF (S-OPF);
2. Maximize a Hopf bifurcation index: an indirect measure of the distance to the Hopf bifurcation point is used as the objective function to be maximized. Using this strategy, two optimization problems are proposed: Eigenvalue Index (EVI) and Singular Value Index (SVI) optimization.

The mathematical formulation of each optimization problem is presented in this chapter, preceded by a discussion on the generalized eigenvalue problem, which forms the basis of all the proposed optimization problems.

## 4.2 Generalized Eigenvalue Problem

A generalized eigenvalue (GE) problem [41] is presented in this section and it is shown that the eigenvalues of this problem are identical to the eigenvalues of the reduced Jacobian matrix,  $J_{\text{reduced}}$ .

As explained in Section 3.2, the small-disturbance stability of a differential-algebraic system can be determined by the eigenvalues of the reduced Jacobian matrix:

$$\mathbf{J}_{\text{reduced}} = \mathbf{J}_1 - \mathbf{J}_2 \mathbf{J}_4^{-1} \mathbf{J}_3 \quad (4.1)$$

where the symbols  $\mathbf{J}_1$ ,  $\mathbf{J}_2$ ,  $\mathbf{J}_3$  and  $\mathbf{J}_4$ , as defined in Section 3.2, are:

- $D$  and  $A$  are the number of the differential (or state) and algebraic variables in the system respectively,
- $\mathbf{J}_1 \in \mathbb{R}^{D \times D}$  is the partial derivative of the system differential equations with respect to the dynamic (or state) variables, i.e.  $\mathbf{J}_1 = \frac{\partial \mathbf{F}(\mathbf{x}, \mathbf{y}; \lambda, \mathbf{p})}{\partial \mathbf{x}}$ ,
- $\mathbf{J}_2 \in \mathbb{R}^{D \times A}$  is the partial derivative of the system differential equations with respect to the algebraic variables, i.e.  $\mathbf{J}_2 = \frac{\partial \mathbf{F}(\mathbf{x}, \mathbf{y}; \lambda, \mathbf{p})}{\partial \mathbf{y}}$ ,
- $\mathbf{J}_3 \in \mathbb{R}^{A \times D}$  is the partial derivative of the system algebraic equations with respect to the dynamic (or state) variables, i.e.  $\mathbf{J}_3 = \frac{\partial \mathbf{G}(\mathbf{x}, \mathbf{y}; \lambda, \mathbf{p})}{\partial \mathbf{x}}$ ,
- $\mathbf{J}_4 \in \mathbb{R}^{A \times A}$  is the partial derivative of the system algebraic equations with respect to the algebraic variables, i.e.  $\mathbf{J}_4 = \frac{\partial \mathbf{G}(\mathbf{x}, \mathbf{y}; \lambda, \mathbf{p})}{\partial \mathbf{y}}$ ,

Consider the following generalized eigenvalue problem:

$$\underbrace{\begin{bmatrix} \mathbf{J}_1 & \mathbf{J}_2 \\ \mathbf{J}_3 & \mathbf{J}_4 \end{bmatrix}}_{\mathbf{J}} \mathbf{v} = \eta \begin{bmatrix} \mathbf{I} & \mathbf{0} \\ \mathbf{0} & \mathbf{0} \end{bmatrix} \mathbf{v} \quad (4.2)$$

where  $\mathbf{J}$  is the full Jacobian matrix of the system,  $\eta \in \mathbb{C}$  is an eigenvalue of this generalized eigenproblem, and  $\mathbf{v} \in \mathbb{C}^{D+A}$  is the right eigenvector associated with the eigenvalue  $\eta$ . Matrix  $\mathbf{I}$  is an identity matrix of proper size,  $\mathbf{I} \in \mathbb{R}^{D \times D}$ .

The characteristic equation of (4.2) is given by:

$$\det \begin{bmatrix} (\mathbf{J}_1 - \eta \mathbf{I}) & \mathbf{J}_2 \\ \mathbf{J}_3 & \mathbf{J}_4 \end{bmatrix} = 0 \quad (4.3)$$

Applying Schur's determinant identity [8], the previous expression can be written as:

$$\det \mathbf{J}_4 \det [(\mathbf{J}_1 - \mathbf{J}_2 \mathbf{J}_4^{-1} \mathbf{J}_3) - \eta \mathbf{I}] = 0 \quad (4.4)$$

where  $\mathbf{J}_4$  is assumed nonsingular. Substituting (4.1) in the preceding equation yields:

$$\det [\mathbf{J}_{\text{reduced}} - \eta \mathbf{I}] = 0 \quad (4.5)$$

Therefore,  $\eta$  is an eigenvalue of the generalized eigenvalue problem if and only if  $\eta$  is an eigenvalue of  $\mathbf{J}_{\text{reduced}}$ , proving the equivalence of the two problems.

Using the matrix  $\mathbf{J}$  over the reduced Jacobian matrix ( $\mathbf{J}_{\text{reduced}}$ ) in the stability analysis has the advantage of being computationally less expensive and more stable numerically, as it does not require the inverse of matrix  $\mathbf{J}_4$  [41].

### 4.3 Optimization of the Maximum System Loadability (MSL) with Respect to Hopf Bifurcations

The optimization problems presented in this section are formulated based on the classical optimal power flow problem, while adding the characteristics that define the occurrence of Hopf bifurcation as constraints to the problem.

Within this section, three formulations are proposed:

- Generalized Eigenvalue Based Hopf Bifurcation Constrained Optimal Power Flow (GEHB-OPF) problem;

- Critical Eigenvalue Based Hopf Bifurcation Constrained Optimal Power Flow (CEHB-OPF) problem;
- Stability Constrained Optimal Power Flow (S-OPF) problem.

All the proposed optimization problems are based on the assumption that the loading pattern of the system is fixed, that is, all the induction motor loads are varied equally, as explained in Section 2.4.5. Hence, the loading parameter  $\lambda \in \mathbb{R}$  represents the incremental load changes. In this case, maximizing the system loadability is equivalent to the maximizing the loading parameter  $\lambda$ .

The general concept of the proposed optimization problem formulations, within the MSL category, may be described as follows:

- Objective:
  - Maximize the loading parameter  $\lambda$ .
- Constraints:
  - System equations at equilibrium: power flow equations, steady-state dynamical model;
  - Operational limits: lower and upper bounds on the bus voltage magnitudes;
  - Controllable parameters limits: lower and upper bounds on the generated active power, as well as the reference voltage of each LTC transformer;
  - HB condition: the system is experiencing a Hopf bifurcation at the maximum  $\lambda$ .

The HB condition is valid for the GEHB-OPF and CEHB-OPF problems. In these cases, the maximum loading parameter is designated by  $\lambda_{\text{HB}}$ , to emphasize that the maximum loadability of the system corresponds to the occurrence of a Hopf bifurcation.

However, in the S-OPF problem, the HB condition is replaced by a less restrictive inequality constraint, as follows:

- Stability constraint: the critical eigenvalue of the system at the maximum loading parameter has a zero or negative real part. Note that, if the optimization program converges to an optimal solution with negative value of  $\alpha$ , then the system is not exhibiting a Hopf or a saddle-node bifurcation.

The mathematical formulation as well as discussion on each problem are presented in the following sections.

#### 4.3.1 Generalized Eigenvalue Based Hopf Bifurcation Constrained Optimal Power Flow (GEHB-OPF) Problem

The GEHB-OPF includes the generalized eigenvalue problem as an equality constraint. It is necessary to separate the real and imaginary parts of (4.2), prior to the inclusion of the generalized eigenproblem into the GEHB-OPF problem. Define  $\alpha \in \mathbb{R}$  and  $\beta \in \mathbb{R}$  as the real and imaginary components of the eigenvalue  $\eta$ , i.e.  $\eta = \alpha + j\beta$ , and

$$\mathbf{v} = \begin{bmatrix} \mathbf{v}_{1\text{R}} + j\mathbf{v}_{1\text{I}} \\ \mathbf{v}_{2\text{R}} + j\mathbf{v}_{2\text{I}} \end{bmatrix}$$

where

- $\mathbf{v}_{1R} \in \mathbb{R}^D$  is the the real portion of the eigenvector  $\mathbf{v}$  that corresponds to the state variables,
- $\mathbf{v}_{1I} \in \mathbb{R}^D$  is the the imaginary portion of the eigenvector  $\mathbf{v}$  that corresponds to the state variables,
- $\mathbf{v}_{2R} \in \mathbb{R}^A$  is the the real portion of the eigenvector  $\mathbf{v}$  that corresponds to the algebraic variables,
- $\mathbf{v}_{2I} \in \mathbb{R}^A$  is the the imaginary portion of the eigenvector  $\mathbf{v}$  that corresponds to the algebraic variables.

Therefore, (4.2) can be rearranged as:

$$\begin{bmatrix} \mathbf{J}_1 & \mathbf{J}_2 \\ \mathbf{J}_3 & \mathbf{J}_4 \end{bmatrix} \begin{bmatrix} \mathbf{v}_{1R} + j\mathbf{v}_{1I} \\ \mathbf{v}_{2R} + j\mathbf{v}_{2I} \end{bmatrix} = (\alpha + j\beta) \begin{bmatrix} \mathbf{v}_{1R} + j\mathbf{v}_{1I} \\ \mathbf{0} \end{bmatrix} \quad (4.6)$$

Separating the real and imaginary components and rearranging (4.6) yields:

$$\begin{bmatrix} \mathbf{J}_1 & \mathbf{J}_2 \\ \mathbf{J}_3 & \mathbf{J}_4 \end{bmatrix} \begin{bmatrix} \mathbf{v}_{1R} \\ \mathbf{v}_{2R} \end{bmatrix} - \alpha \begin{bmatrix} \mathbf{v}_{1R} \\ \mathbf{0} \end{bmatrix} + \beta \begin{bmatrix} \mathbf{v}_{1I} \\ \mathbf{0} \end{bmatrix} = \mathbf{0} \quad (4.7)$$

$$\begin{bmatrix} \mathbf{J}_1 & \mathbf{J}_2 \\ \mathbf{J}_3 & \mathbf{J}_4 \end{bmatrix} \begin{bmatrix} \mathbf{v}_{1I} \\ \mathbf{v}_{2I} \end{bmatrix} - \alpha \begin{bmatrix} \mathbf{v}_{1I} \\ \mathbf{0} \end{bmatrix} - \beta \begin{bmatrix} \mathbf{v}_{1R} \\ \mathbf{0} \end{bmatrix} = \mathbf{0} \quad (4.8)$$

The GEHB-OPF problem can then be formulated as follows:

**objective function:**

$$\max \quad \lambda_{HB}$$

subject to:

$$\mathbf{F}(\mathbf{x}, \mathbf{y}; \lambda_{\text{HB}}, \mathbf{p}) = \mathbf{0} \quad (4.9)$$

$$\mathbf{G}(\mathbf{x}, \mathbf{y}; \lambda_{\text{HB}}, \mathbf{p}) = \mathbf{0} \quad (4.10)$$

$$\mathbf{J} \begin{bmatrix} \mathbf{v}_{1r} \\ \mathbf{v}_{2r} \end{bmatrix} - \alpha \begin{bmatrix} \mathbf{v}_{1r} \\ \mathbf{0} \end{bmatrix} + \beta \begin{bmatrix} \mathbf{v}_{1i} \\ \mathbf{0} \end{bmatrix} = \mathbf{0} \quad (4.11)$$

$$\mathbf{J} \begin{bmatrix} \mathbf{v}_{1i} \\ \mathbf{v}_{2i} \end{bmatrix} - \alpha \begin{bmatrix} \mathbf{v}_{1i} \\ \mathbf{0} \end{bmatrix} - \beta \begin{bmatrix} \mathbf{v}_{1r} \\ \mathbf{0} \end{bmatrix} = \mathbf{0} \quad (4.12)$$

$$\left\| \begin{bmatrix} \mathbf{v}_{1r} \\ \mathbf{v}_{2r} \end{bmatrix} \right\|_2^2 = 1 \quad (4.13)$$

$$\left\| \begin{bmatrix} \mathbf{v}_{1i} \\ \mathbf{v}_{2i} \end{bmatrix} \right\|_2^2 = 1 \quad (4.14)$$

$$\alpha = 0 \quad (4.15)$$

$$\beta^2 > 0 \quad (4.16)$$

$$\underline{\mathbf{p}} \leq \mathbf{p} \leq \bar{\mathbf{p}} \quad (4.17)$$

$$\underline{\mathbf{h}} \leq \mathbf{h}(\mathbf{y}) \leq \bar{\mathbf{h}} \quad (4.18)$$

where

- $\lambda_{\text{HB}}$ : loading parameter at the Hopf bifurcation point,
- $\mathbf{x} \in \mathbb{R}^D$ : vector of state variables (rotor and stator flux linkage per second along the “ $d$ ” and “ $q$ ” axis, and speed of the rotor for each induction motor, the tap setting for each LTC transformer),
- $\mathbf{y} \in \mathbb{R}^A$ : vector of algebraic variables, including real and imaginary components

of bus voltages, stator terminal voltage of the induction motors, active and reactive power consumed by the motors, active and reactive power transferred by the LTC transformers, reactive power generation in the system and the active power of the slack bus,

- $\mathbf{p} \in \mathbb{R}^{CP}$ : vector of controllable parameters. In this experiment, the controllable parameters are magnitude of the voltage at the generator buses, real voltage of the slack bus (the imaginary component of the slack bus voltage is set to zero, thus corresponding to the reference angle equal to zero), reference voltage of each LTC transformer, and the active generated power at the generator buses,
- $\underline{\mathbf{p}}, \overline{\mathbf{p}}$ : lower and upper bounds for the controllable parameters,
- $\underline{\mathbf{h}}, \overline{\mathbf{h}}$ : lower and upper bounds for the voltage magnitude at each bus
- $\mathbf{h} : \mathbb{R}^A \rightarrow \mathbb{R}^L$ : represents the voltage magnitude at each uncontrolled voltage buses where  $L$  is the total number of the uncontrolled voltage buses.

and the constraints

- (4.9): represents the dynamic equations of the system set to zero to find the equilibrium point,
- (4.10): represents the power flow equations at each bus, and the algebraic equations that links the induction motors and LTC transformers in the system to the power flow equations,
- (4.11) and (4.12): represent the generalized eigenvalue problem,



- (4.13) and (4.14): enforce the nonzero condition on the eigenvector associated with the eigenvalue  $\eta$ ,
- (4.15) and (4.16): enforce the Hopf point conditions,
- (4.17): represents the minimum and maximum limits on the controllable parameters,
- (4.18): represents the lower and upper limits on the magnitude of the voltage at each bus

The GEHB-OPF optimization problem is smooth, that is, the objective function and all the constraints of the problem are continuous and differentiable with respect to the optimization variables.

A drawback of this formulation is that the criticality of the eigenvalue under consideration in this optimization problem is not enforced. It is expected that, by initializing the optimization method with a good initial solution, the optimal solution will model an eigenvalue variable that represents the critical eigenvalue of the system. Therefore, this method is effectively a heuristic method, since there is no guarantee that the maximum obtained by the optimization procedure is the actual maximum.

#### **4.3.2 Critical Eigenvalue Based Hopf Bifurcation Constrained Optimal Power Flow (CEHB-OPF) Problem**

The CEHB-OPF problem differs from the GEHB-OPF problem in that the CEHB-OPF problem utilizes the critical eigenvalue of the reduced Jacobian matrix (i.e. the rightmost eigenvalue of the system) in order to define the Hopf bifurcation point.

The critical eigenvalue of the generalized eigenvalue problem is a complex valued function of the optimization variables, denoted by  $\eta(\mathbf{x}, \mathbf{y}, \lambda_{\text{HB}}, \mathbf{p})$ , and it is computed as follows:

1. The full Jacobian matrix  $\mathbf{J}$  of the system is computed;
2. The generalized eigenvalue problem is solved, that is, all the eigenvalues of the system are obtained;
3. The complex value returned by the function  $\eta(\mathbf{x}, \mathbf{y}, \lambda_{\text{HB}}, \mathbf{p})$  is the eigenvalue with the largest real part.

The mathematical formulation of the CEHB-OPF problem is given below:  
**objective function:**

$$\max \lambda_{\text{HB}}$$

**subject to:**

$$\mathbf{F}(\mathbf{x}, \mathbf{y}; \lambda_{\text{HB}}, \mathbf{p}) = \mathbf{0} \quad (4.19)$$

$$\mathbf{G}(\mathbf{x}, \mathbf{y}; \lambda_{\text{HB}}, \mathbf{p}) = \mathbf{0} \quad (4.20)$$

$$\text{Re}\{\eta(\mathbf{x}, \mathbf{y}; \lambda_{\text{HB}}, \mathbf{p})\} = 0 \quad (4.21)$$

$$\text{Im}\{\eta(\mathbf{x}, \mathbf{y}; \lambda_{\text{HB}}, \mathbf{p})\}^2 > 0 \quad (4.22)$$

$$\underline{\mathbf{p}} \leq \mathbf{p} \leq \bar{\mathbf{p}} \quad (4.23)$$

$$\underline{\mathbf{h}} \leq \mathbf{h}(\mathbf{y}) \leq \bar{\mathbf{h}} \quad (4.24)$$

where the real and imaginary components of the function  $\eta(\cdot)$  are employed in equations (4.21) and (4.22) to define the Hopf bifurcation condition. It should be noted

that the real part of the critical eigenvalue is not a smooth function of the optimization variables, thus the CEHB-OPF problem is not smooth [53].

#### 4.3.3 Stability Constrained Optimal Power Flow (S-OPF) Problem

In the previous optimization problems (GEHB-OPF and CEHB-OPF), the system at the maximum loading parameter is necessarily experiencing a Hopf bifurcation. If there is no possibility of a Hopf bifurcation in the system (e.g., when the only dynamical element of the power network is a LTC transformer), it is not possible to achieve feasibility in the GEHB-OPF and CEHB-OPF problems. The S-OPF formulation circumvents this problem by softening the Hopf bifurcation condition, as shown in this section.

As in the CEHB-OPF problem, let  $\eta(\mathbf{x}, \mathbf{y}, \lambda_c, \mathbf{p})$  be the critical eigenvalue of the system as a function of the optimization variables, where  $\lambda_c$  is the maximum value of the loading parameter.

The S-OPF optimization problem is formulated as follows:

**objective function:**

$$\max \quad \lambda_c$$

**subject to:**

$$\mathbf{F}(\mathbf{x}, \mathbf{y}; \lambda_c, \mathbf{p}) = \mathbf{0} \quad (4.25)$$

$$\mathbf{G}(\mathbf{x}, \mathbf{y}; \lambda_c, \mathbf{p}) = \mathbf{0} \quad (4.26)$$

$$\text{Re}\{\eta(\mathbf{x}, \mathbf{y}; \lambda_c, \mathbf{p})\} \leq 0 \quad (4.27)$$

$$\underline{\mathbf{p}} \leq \mathbf{p} \leq \bar{\mathbf{p}} \quad (4.28)$$

$$\underline{\mathbf{h}} \leq \mathbf{h}(\mathbf{y}) \leq \bar{\mathbf{h}} \quad (4.29)$$

Let  $\alpha = \text{Re}\{\eta(\mathbf{x}, \mathbf{y}; \lambda_c, \mathbf{p})\}$  and  $\beta = \text{Im}\{\eta(\mathbf{x}, \mathbf{y}; \lambda_c, \mathbf{p})\}$ . As shown in equation (4.27),  $\alpha$  is constrained to be less or equal to zero, implying an optimal system that presents one of the following situations, at the maximum loading parameter:

- a) The system is stable and away from bifurcation, if the optimizer converges to a solution where  $\alpha < 0$ .
- b) The system is at the point of Hopf bifurcation, if the optimizer converges to a solution where  $\alpha = 0$  and  $\beta \neq 0$ .
- c) The system is at the point of saddle-node bifurcation, if the optimizer converges to a solution where  $\alpha = 0$  and  $\beta = 0$ ;

Observe that the S-OPF problem is more general than the GEHB-OPF and the GEHB-OPF problems, since the S-OPF problem incorporates the possible solutions of the GEHB-OPF and CEHB-OPF problems as the subcase (b) in the above listing.

#### 4.4 Optimization of a Hopf Bifurcation Index

The optimization of the maximum system loadability assumes that all the loads change simultaneously, and at the same rate, i.e., a fixed loading direction is given. However, in reality, the different loads in the system can be independent. Thus, a better assumption to the maximum loadability problem would be to employ a vector of loading parameters to describe each load separately, rather than a single value. Such approach implies an increase in the dimensionality of the system, and the added computational cost might render this formulation unattractive.

The increase in the dimensionality of the optimization problem can be avoided by the adoption of an indirect measure of the distance to bifurcation. In the work presented in [19], the authors proposed the utilization of several indices to detect and predict instabilities associated with Hopf and saddle-node bifurcations. These indices can be perceived as an indirect measure of the distance to bifurcation.

In this section, the usage of two indices to bifurcation – the Eigenvalue Index (EVI) and the Singular Value Index (SVI) – as cost functions in optimal power flow problems is proposed. The EVI and SVI have been previously introduced in Section 3.4.1

#### 4.4.1 Eigenvalue Index Optimization problem

The EVI optimization problem is formulated as follows:

**objective function:**

$$\max \quad -\operatorname{Re}\{\eta(\mathbf{x}, \mathbf{y}; \lambda_0, \mathbf{p})\}$$

**subject to:**

$$\mathbf{F}(\mathbf{x}, \mathbf{y}; \lambda_0, \mathbf{p}) = \mathbf{0} \quad (4.30)$$

$$\mathbf{G}(\mathbf{x}, \mathbf{y}; \lambda_0, \mathbf{p}) = \mathbf{0} \quad (4.31)$$

$$\underline{\mathbf{p}} \leq \mathbf{p} \leq \bar{\mathbf{p}} \quad (4.32)$$

$$\underline{\mathbf{h}} \leq \mathbf{h}(\mathbf{y}) \leq \bar{\mathbf{h}} \quad (4.33)$$

where  $\eta(\mathbf{x}, \mathbf{y}; \lambda_0, \mathbf{p})$  is the critical eigenvalue of the system and  $\lambda_0$  represents the value of  $\lambda$  at the normal operating point. Observe that, in contrary to the optimum system loadability approaches, the loading parameter  $\lambda$  is not an optimization variable in this mathematical formulation.

The motivation for the proposal of the EVI optimization problem comes from the fact that the real part of the critical eigenvalue (denoted by  $\alpha$ ) can be considered as a measure of the small-disturbance stability of the power network, since it dictates the asymptotic exponential rate of decay of perturbations in the system. It is implicitly hypothesized that a larger stability (i.e., a smaller  $\alpha$ ) corresponds to a larger loading margin.

#### 4.4.2 Singular Value Index Optimization problem

The minimum singular value of the modified reduced Jacobian matrix ( $\mathbf{J}_{\text{reduced}}$ ) can be used as an index to detect Hopf bifurcations, as shown in Section 3.4.1. However, this method requires an inverse matrix computation. Such expensive computation can be avoided by using the minimum singular value of a modified full Jacobian matrix as proposed in [19] and explained below.

Consider the generalized eigenvalue problem separated into real and imaginary components as given by (4.7) and (4.8) and restated below:

$$\begin{bmatrix} \mathbf{J}_1 & \mathbf{J}_2 \\ \mathbf{J}_3 & \mathbf{J}_4 \end{bmatrix} \begin{bmatrix} \mathbf{v}_{1R} \\ \mathbf{v}_{2R} \end{bmatrix} - \alpha \begin{bmatrix} \mathbf{v}_{1R} \\ \mathbf{0} \end{bmatrix} + \beta \begin{bmatrix} \mathbf{v}_{1I} \\ \mathbf{0} \end{bmatrix} = \mathbf{0} \quad (4.34)$$

$$\begin{bmatrix} \mathbf{J}_1 & \mathbf{J}_2 \\ \mathbf{J}_3 & \mathbf{J}_4 \end{bmatrix} \begin{bmatrix} \mathbf{v}_{1I} \\ \mathbf{v}_{2I} \end{bmatrix} - \alpha \begin{bmatrix} \mathbf{v}_{1I} \\ \mathbf{0} \end{bmatrix} - \beta \begin{bmatrix} \mathbf{v}_{1R} \\ \mathbf{0} \end{bmatrix} = \mathbf{0} \quad (4.35)$$

Combining the two equations (4.34) and (4.35) yields:

$$\left( \underbrace{\begin{bmatrix} \mathbf{J}_1 & \mathbf{J}_2 & \beta \mathbf{I}_n & \mathbf{0} \\ \mathbf{J}_3 & \mathbf{J}_4 & \mathbf{0} & \mathbf{0} \\ -\beta \mathbf{I}_n & \mathbf{0} & \mathbf{J}_1 & \mathbf{J}_2 \\ \mathbf{0} & \mathbf{0} & \mathbf{J}_3 & \mathbf{J}_4 \end{bmatrix}}_{\mathbf{J}_m} - \alpha \begin{bmatrix} \mathbf{I}_n & \mathbf{0} & \mathbf{0} & \mathbf{0} \\ \mathbf{0} & \mathbf{0} & \mathbf{0} & \mathbf{0} \\ \mathbf{0} & \mathbf{0} & \mathbf{I}_n & \mathbf{0} \\ \mathbf{0} & \mathbf{0} & \mathbf{0} & \mathbf{0} \end{bmatrix} \right) \begin{bmatrix} \mathbf{v}_{1R} \\ \mathbf{v}_{2R} \\ \mathbf{v}_{1I} \\ \mathbf{v}_{2I} \end{bmatrix} = \mathbf{0} \quad (4.36)$$

where  $\mathbf{J}_m$  is the modified full Jacobian matrix of the system. Notice that at the Hopf bifurcation point the real component of the critical eigenvalue becomes zero, i.e.  $\alpha = 0$ . Therefore, matrix  $\mathbf{J}_m$  becomes singular since the eigenvectors are nonzero. In this case, the minimum singular value of matrix  $\mathbf{J}_m$  is zero.

In the SVI optimization problem, the objective is to maximize the minimum singular value  $\sigma_{\min}$  of the modified Jacobian matrix, as presented below:

**objective function:**

$$\max \quad \sigma_{\min}(\mathbf{J}_m)$$

**subject to:**

$$\mathbf{F}(\mathbf{x}, \mathbf{y}; \lambda_0, \mathbf{p}) = \mathbf{0} \quad (4.37)$$

$$\mathbf{G}(\mathbf{x}, \mathbf{y}; \lambda_0, \mathbf{p}) = \mathbf{0} \quad (4.38)$$

$$\underline{\mathbf{p}} \leq \mathbf{p} \leq \overline{\mathbf{p}} \quad (4.39)$$

$$\underline{\mathbf{h}} \leq \mathbf{h}(\mathbf{y}) \leq \overline{\mathbf{h}} \quad (4.40)$$

This problem is less direct than the EVI optimization, but is considered more robust and well behaved, since singular values are less sensitive to small imprecision in the matrix  $\mathbf{J}_m$  [41].

## 4.5 Summary

In this chapter the following optimization problems are proposed to maximize the system loading margin with respect to the occurrence of Hopf bifurcation:

- 1- Generalized Eigenvalue Based Hopf Bifurcation Constrained Optimal Power Flow (GEHB-OPF) problem,
- 2- Critical Eigenvalue Based Hopf Bifurcation Constrained Optimal Power Flow (CEHB-OPF) problem,
- 3- Stability Constrained Optimal Power Flow (S-OPF) problem,
- 4- Eigenvalue Index Optimization (EVI) problem
- 5- Singular Value Index optimization (EVI) problem,

In the first three problems, the system loadability is directly maximized, whereas in the last two problems it is attempted to improve the system maximum loadability through maximization of an indirect measure of the distance to the bifurcation point. The advantage and disadvantage of each method is briefly mentioned below:

- GEHB-OPF problem: the optimization problem is smooth; however, the criticality of the eigenvalue modeled in the problem is not enforced, which renders the method an heuristic approach. The Hopf bifurcation point is implicitly modeled and a loading direction is assumed.
- CEHB-OPF problem: the criticality of the modeled eigenvalue is enforced. However, the critical eigenvalue is not a smooth function of the optimization



variables. The Hopf bifurcation point is implicitly modeled and a loading direction is assumed.

- S-OPF problem: the Hopf bifurcation constraint is softened to increase the feasibility region. A loading direction is assumed.
- EVI optimization problem: no loading direction is required. The optimal solution does not guarantee an effectively improved loading margin. It is worth mentioning that the eigenvalues of the system are highly sensitive to matrix perturbations when the Jacobian matrix of the system is a poorly conditioned matrix [41].
- SVI optimization problem: no loading direction is required. The singular values of a matrix are more robust to matrix perturbations as compared to the eigenvalues [41]. The optimal solution does not guarantee an effectively improved loading margin.

# Chapter 5

## Numerical Analysis

### 5.1 Introduction

This chapter presents the numerical results of the proposed optimization problems described in Chapter 4. The following test systems are employed to demonstrate the characteristics of the proposed problems:

- A 3-bus test system with an infinite bus and a LTC transformer connected to an induction motor, depicted in Figure 5.1

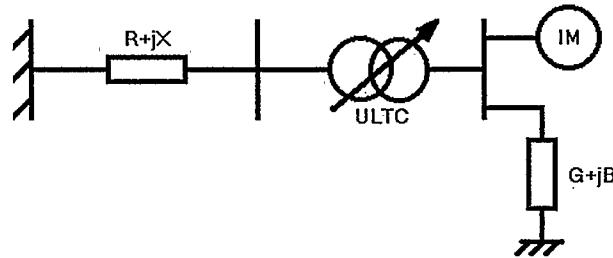


Figure 5.1: Schematic diagram of the 3-bus test system

- A 14-bus test system based on IEEE 14-bus test system. The IEEE standard

14 bus test case is modified to employ a LTC transformer between the buses 5 and 6 as shown in Figure 5.2. Furthermore, an induction motor is connected to bus 13. The modified network contains 2 generators and 2 synchronous condensers.

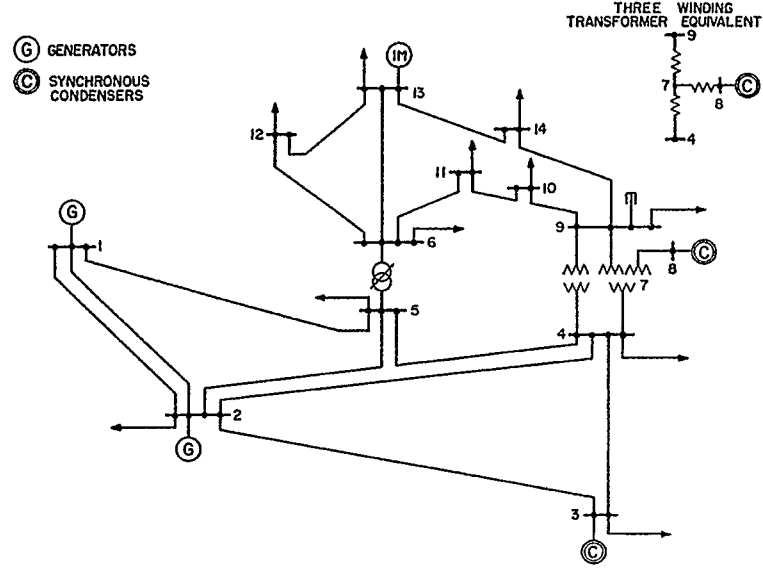


Figure 5.2: Schematic diagram of 14-bus test system [54]

In all cases, a continuation method is used to trace the voltage profiles of the systems under investigation for the initial and optimal values of the controllable parameters.

## 5.2 Effect of the Controllable Parameters in the Loading Margin of the 3-Bus Test System

The 3-bus test system has only two controllable parameters: the reference voltage of the LTC transformer ( $V_{ref}$ ), and the voltage magnitude at the slack bus ( $V_{slack}$ ).

In such a simple system, it is possible to perform an exhaustive investigation of the maximum  $\lambda$  as a function of  $V_{\text{ref}}$  and  $V_{\text{slack}}$ , which provides the true optimal solution of this system. The true optimal serves as the basis for comparison of the solution of each proposed optimization problem, giving the opportunity for a better analysis of the obtained results.

Figure 5.3 shows the value of  $\lambda$  as a function of  $V_{\text{ref}}$  and  $V_{\text{slack}}$ , within the operational limits of the controllable parameters. It is noticed that the maximum  $\lambda$  is achieved at  $V_{\text{ref}} = 1.1$  and  $V_{\text{slack}} = 1.1$ . It is also observed that  $\lambda$  is more sensitive to variations in  $V_{\text{ref}}$  than  $V_{\text{slack}}$ . This can be explained by the fact that the induction machine is connected to the secondary of the LTC transformer, thus being directly affected by the LTC's reference voltage, and on a lesser scale by the slack bus voltage.

The development of bifurcation in the system is a consequence of the interaction between the dynamics of the induction machine and that of the LTC transformer. Therefore,  $V_{\text{ref}}$  has more impact in the occurrence of bifurcation than  $V_{\text{slack}}$ , as mentioned before. Figure 5.4 illustrates the effect of changing  $V_{\text{slack}}$  when  $V_{\text{ref}}$  is kept fixed at 1.0 p.u., and it is seen that  $\lambda$  does not change significantly. In contrary, Figure 5.5 shows that a large variation in  $\lambda$  is obtained when  $V_{\text{ref}}$  is altered and  $V_{\text{slack}}$  is kept at 1 P.U.

It should be noted that these results cannot be directly generalized to larger systems. Nevertheless, the insight obtained from the discussion on this simple test system is useful in the comprehension of more complex systems.

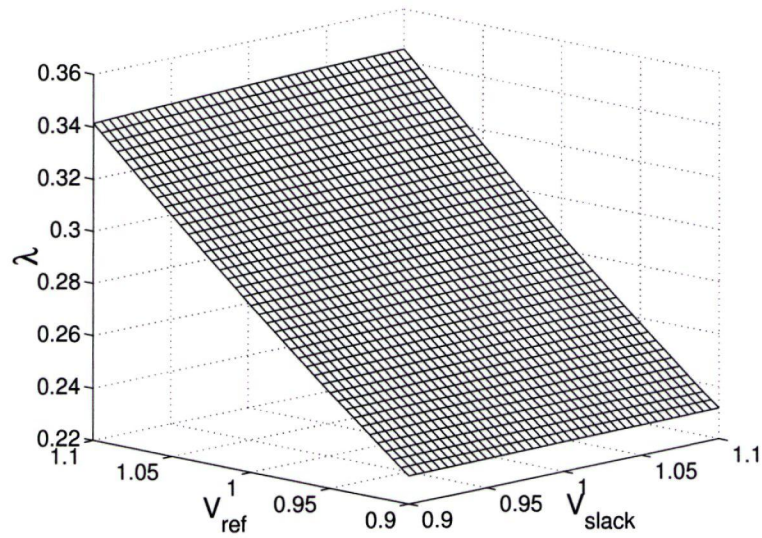


Figure 5.3: The maximum loading parameter  $\lambda$  as a function of the voltage reference of the LTC transformer ( $V_{ref}$ ) and the slack bus voltage ( $V_{slack}$ ) for the '3-bus' test system.

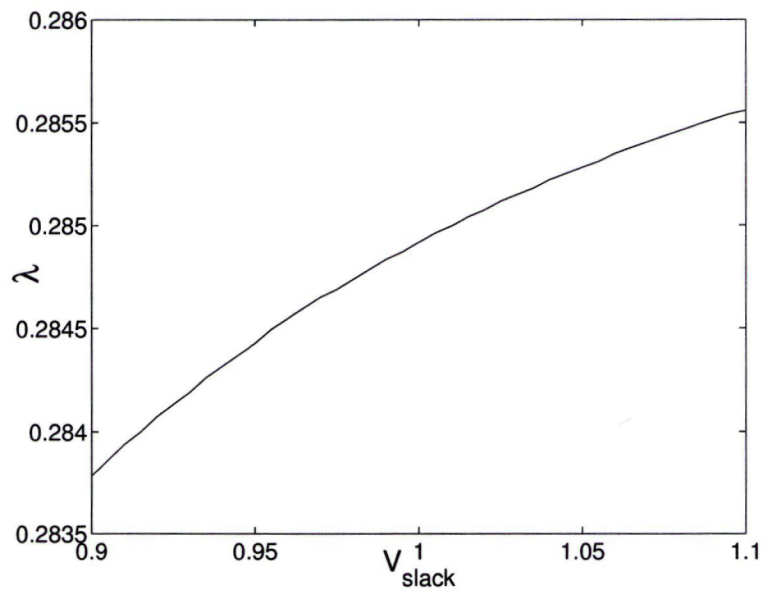


Figure 5.4: The maximum loading parameter  $\lambda$  as a function of the slack bus voltage ( $V_{slack}$ ) for the '3-bus' test system. The reference voltage of the LTC transformer is fixed at 1.0 P.U.

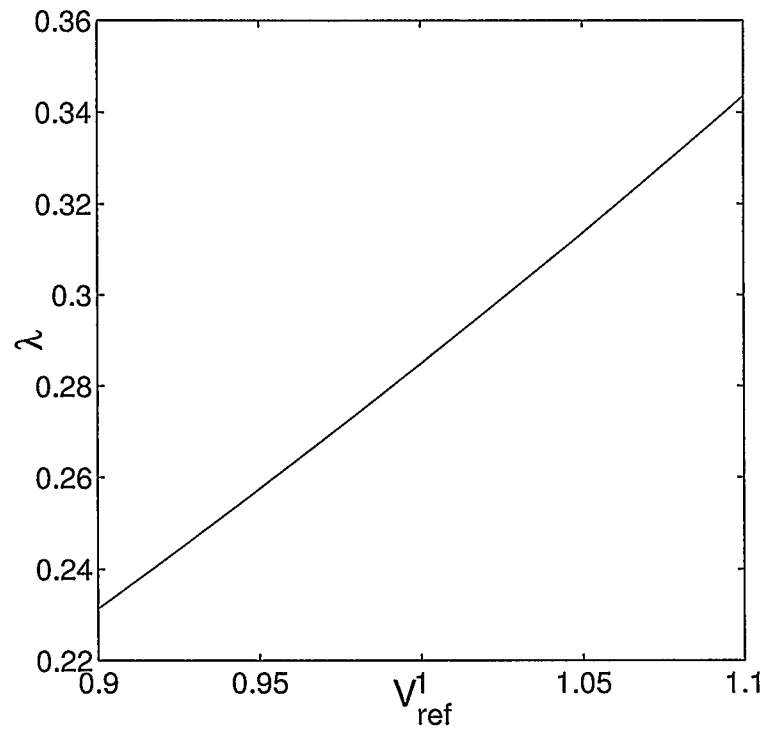


Figure 5.5: The maximum loading parameter  $\lambda$  as a function of the voltage reference of the LTC transformer ( $V_{\text{ref}}$ ) for the ‘3-bus’ test system. The slack bus voltage is fixed at 1.0 P.U.

## 5.3 Results of the Optimization Problems

### 5.3.1 Generalized Eigenvalue Based HB Constrained OPF (GEHB-OPF) Problem

The GEHB-OPF problem, presented in Section 4.3.1, is formulated as the maximization of the loading parameter  $\lambda_{HB}$  at the HB point, satisfying the following conditions: system state equations at rest (or equilibrium); algebraic equations; system limits; the generalized eigenvalue problem; and the stability condition imposed on a complex eigenvalue  $\alpha + j\beta$  of the mentioned generalized eigenvalue problem, that is,  $\alpha = 0$  and  $\beta^2 > 0$ .

A valid optimal solution, in terms of the stability of the power system under investigation, is a solution where all the eigenvalues of the reduced Jacobian matrix (or equivalently, the eigenvalues of the generalized eigenvalue problem) are in the left half-plane of the complex plane, except for the pair of complex conjugate eigenvalues that are placed on the imaginary axis, characterizing the occurrence of Hopf bifurcation. Therefore, the system eigenvalue ( $\alpha + j\beta$ ) that appears in the GEHB-OPF problem and its complex conjugate ( $\alpha - j\beta$ ) must be the right most eigenvalue of the system in order to obtain a valid solution.

However, in the GEHB-OPF problem, the referred criticality condition of the eigenvalue is not enforced. The heuristic approach to maintain the validity of the optimization results is to initialize the eigenvalue variables as the critical eigenvalue of the reduced Jacobian matrix, at the HB point, with the initial set of controllable parameters. As the solver evolves, we expect the validity of the solution to be conserved, although such assertion cannot be guaranteed.

The optimization formulation is implemented in the AMPL package. The solver LOQO, which is based on the logarithmic barrier interior point method, is employed to find the optimal solution of the problem. The optimization procedure is initialized at the HB point, with the initial set of controllable parameters. This initial HB point is obtained by a sequential Newton-Raphson (SNR) search, that is, the Newton-Raphson method is used to find the equilibrium point of the system for successive values of  $\lambda$  until the HB point is detected. It is worth mentioning that the sequential Newton-Raphson search method is a computationally expensive procedure for large systems, if thought of as a part of an online system stability analysis tool. Since the optimization problems discussed in this thesis are offline methods to investigate the system stability, the computational cost of the SNR search method does not pose a disadvantage in the present work.

### 3-Bus Test System

The results of the optimization procedure are described using Table 5.1, and Figures 5.6 and 5.7. The solver finds a solution in 22 iterations. At maximum  $\lambda_{HB}$  the solver returns  $\alpha = 0$  and  $\beta = 0.43$ , indicating a HB point. The eigenvalues of the reduced Jacobian matrix of the system are computed in Matlab. It is verified that the optimization eigenvalue variable is indeed representing the critical eigenvalue of the system.

It was observed experimentally that the convergence of this model is highly sensitive to the initialization of optimization variables, which is a major disadvantage of the GEHB-OPF problem.

Table 5.1 shows that in the optimal solution the generator bus voltage and the



reference voltage of the LTC transformer are pushed to their maximum limit in the optimal system. These results agree with the expected optimal results from the exhaustive search, described in Section 5.2. The loading margin is increased by 21% of its original value, indicating a substantial improvement. The enhancement in the loading margin is also exemplified in the voltage profile of bus number 2, shown in Figure 5.6. The lower curve indicates the loading margin of the original system and the upper curve shows the loading margin for the optimal system.

Parameter	Original System	Optimal System
$\lambda_{\text{bifurcation}}$	0.2849	0.344709
$ V_1 $ (slack bus)	1	1.1
$V_{\text{ref}}$ (LTC 1)	1	1.1

Table 5.1: Optimization results for the ‘3-bus’ test system, when solving the GEHB-OPF problem

The movement of the eigenvalues in the complex plane is depicted in Figure 5.7 for the optimal system. All eigenvalues remain in the left half-plane of the complex plane, except for the critical complex conjugate eigenvalue pair that cross the imaginary axis, indicating the occurrence of Hopf bifurcation. This is shown more clearly in Figure 5.8 by enlarging the region where the bifurcation occurs. The initial period of the limit cycle oscillation can be computed as  $T_0 = \frac{2\pi}{\beta}$  and for this system is equal to 14.61 seconds.

The non-critical eigenvalues are associated with rapid exponential decay, since these eigenvalues present real components that are negative, and large in magnitude. Therefore, the transient behavior associated with the non-critical eigenvalues has short duration, and does not impact in the stability analysis of the system.

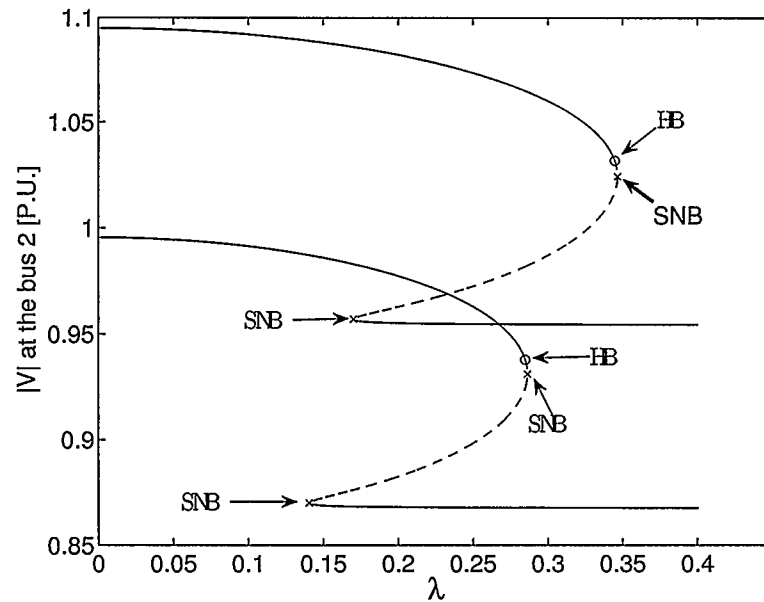


Figure 5.6: Voltage profile of bus 2 in the 3-bus test system, when solving the GEHB-OPF problem. The lower curve indicates the original system and the upper curve represents the optimal system. Bifurcation points are shown for each profile

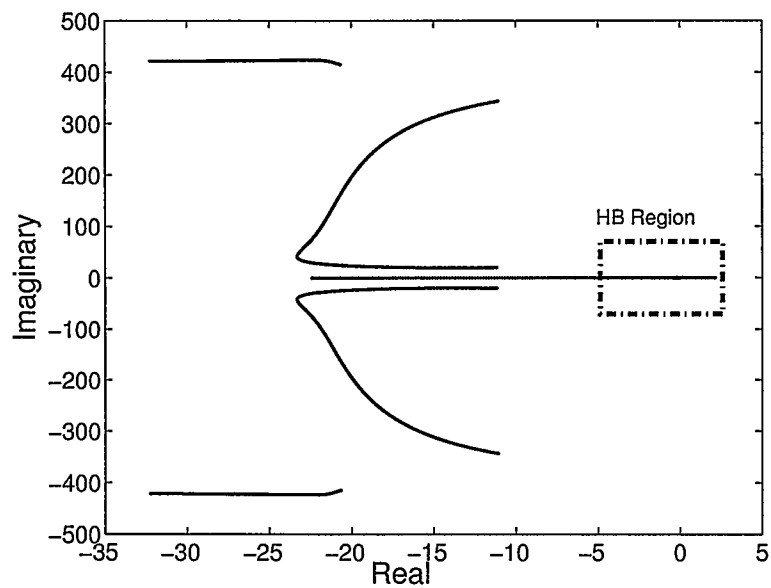


Figure 5.7: Eigenvalue movement in the complex plain, '3-bus' test system, when solving the GEHB-OPF

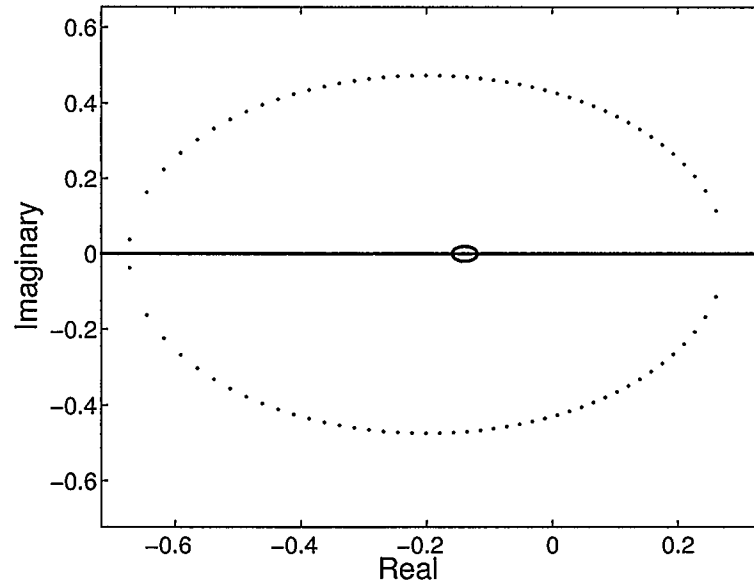


Figure 5.8: Enlargement of the HB region, ‘3-bus’ test system, when solving the GEHB-OPFs

### 14-bus Test System

It was not possible to achieve convergence of the optimization procedure with the 14-bus test system, in this formulation. This fact highlights the main drawback of the approach which is the inability to incorporate the constraints on the critical eigenvalue. In the previous test system, the heuristic method was sufficient to have the solution converge. However, as can be noted in this case, when dealing with even moderately complex systems, the numerical convergence of the GEHB-OPF problem fails.

### 5.3.2 Critical Eigenvalue Based HB Constrained OPF Problem (CEHB-OPF)

The CEHB-OPF problem, introduced in Section 4.3.2, is formulated as the maximization of the loading parameter  $\lambda_{HB}$  at the HB point, satisfying the following conditions: system state equations at rest; algebraic equations; system limits and the HB condition imposed on the *critical* eigenvalue  $\alpha + j\beta$  of the reduced Jacobian matrix, that is,  $\alpha = 0$  and  $\beta^2 > 0$ . The problem is solved using the Matlab optimization toolkit, whose solver is based on a sequential quadratic programming method.

The optimization procedure is initialized at the HB point, with the initial set of controllable parameters, as in the GEHB-OPF problem of Section 5.3.1. Likewise, the initial HB point is obtained by a Sequential Newton-Raphson (SNR) search, implemented in Matlab.

#### 3-Bus Test System

The obtained results, shown in Table 5.2, are equal to the results of the GEHB-OPF problem (Section 5.3.1), and agree with the expected optimal results obtained in the exhaustive optimal search of Section 5.2. The method took 6 iterations to find the optimal solution. The critical eigenvalue at the bifurcation point for the optimal system is given by  $\alpha = 0$  and  $\beta = 0.43$ , indicating a HB point. The initial period of the limit cycle oscillation is  $T_0 = \frac{2\pi}{\beta} = 14.61$  seconds. The voltage profile of bus 2 and eigenvalue movement obtained in the CEHB-OPF problem coincides with that of the GEHB-OPF problem.

Parameter	Original System	Optimal System
$\lambda_{\text{bifurcation}}$	0.284913	0.344709
$ V_1 $ (slack bus)	1.000000	1.100000
$V_{\text{ref}}$ (LTC 1)	1.000000	1.100000

Table 5.2: Optimization results for the ‘3-bus’ test system, when solving the CEHB-OPF problem

### 14-bus Test System

For the 14-bus test system 13 iterations were required to find the optimal solution. The real and imaginary components of the critical eigenvalue for maximum  $\lambda_{\text{HB}}$  are:  $\alpha = 0$  and  $\beta = 0.24$ . The initial period of the limit cycle oscillation is  $T_0 = \frac{2\pi}{\beta} = 26.18$  seconds.

The results are described in Table 5.3. It can be noted that the generator bus voltages and the reference voltage of the LTC transformer are pushed to their maximum limit in the optimal system. This fact is a consequence of the increase in the power consumption of the induction machine, as the loading parameter increases: a larger generated voltage implies a greater availability of power to the load elements of the network. It is also observed in Table 5.3 that the generated power in bus 2 increases, as a response to the larger consumption of power by the induction machine.

The loading margin is improved by 20% of its original value, as depicted in Table 5.3, and illustrated by the voltage profiles of bus 13 with the initial and the optimal set of parameters in Figure 5.9. The voltage profiles are drawn up to the first saddle-node bifurcation (SNB) point. The dynamics of the system past the first SNB point is not of interest for this discussion, and is therefore suppressed for greater clarity. Figure 5.10 represents the movement of the critical pair of eigenvalue in the vicinity of the Hopf bifurcation.

Parameter	Original System	Optimal System
$\lambda_{\text{bifurcation}}$	0.253507	0.305062
$ V_1 $ (slack bus)	1.060000	1.100000
$ V_2 $	1.045000	1.100000
$ V_3 $	1.010000	1.100000
$ V_8 $	1.090000	1.100000
$V_{\text{ref}}$ (LTC 1)	1.000000	1.100000
$P_{\text{gen}}$ (bus 2)	0.400000	0.443671

Table 5.3: Optimization results for ‘IEEE14bus’ test system, when solving the CEHB-OPF problem

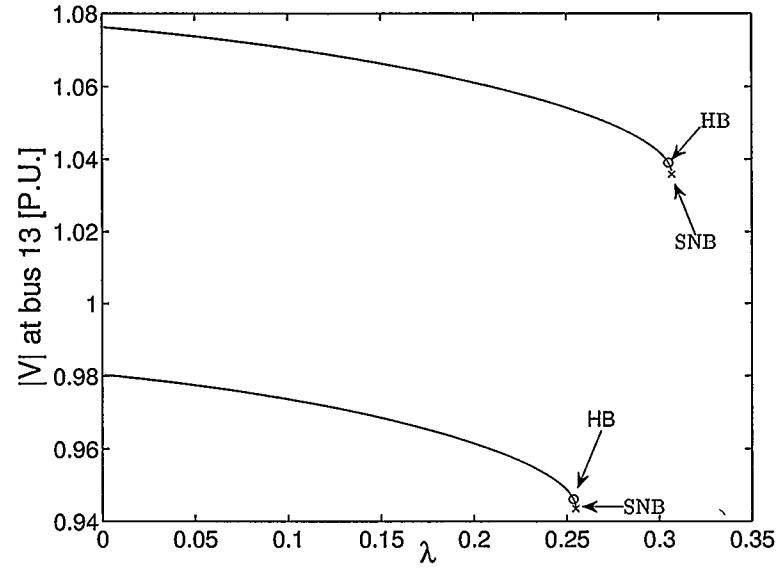


Figure 5.9: Voltage profile of bus 13 in the ‘IEEE14bus’ test system, when solving the CEHB-OPF problem. The lower curve indicates the original system and the upper curve represents the optimal system

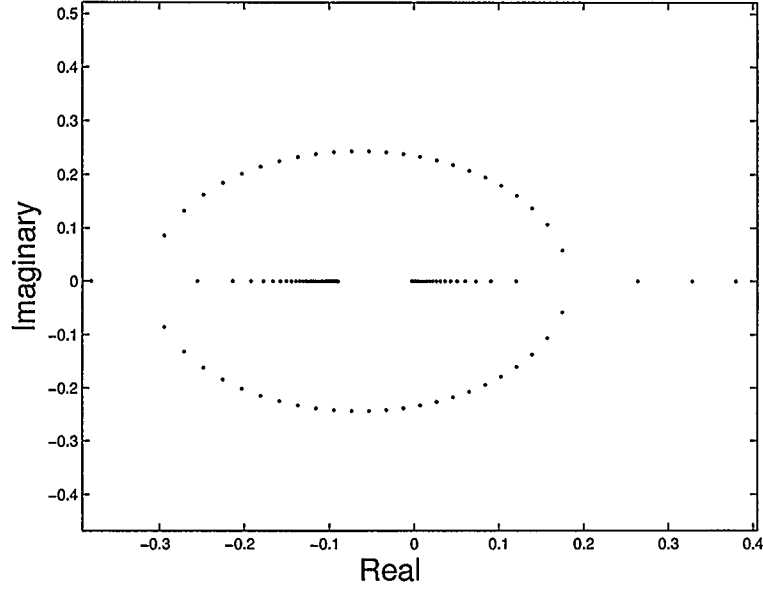


Figure 5.10: Enlargement of the HB region, ‘IEEE14bus’ test system, when solving the CEHB-OPF problem

### 5.3.3 Stability Constrained OPF Problem (S-OPF)

The S-OPF problem, presented in Section 4.3.3, is formulated as the maximization of the loading parameter  $\lambda$  at the system critical point, satisfying the following conditions: system state equations at rest; algebraic equations; system limits; the stability condition imposed on the *critical* eigenvalue  $\alpha + j\beta$  of the reduced Jacobian matrix, that is,  $\alpha \leq 0$ . It is worth mentioning that the feasible space in this problem encompasses the feasible space of the GEHB-OPF and the CEHB-OPF problems. Therefore, it is possible to find an optimal solution of the S-OPF problem that results in a better loading margin than that of the GEHB-OPF and CEHB-OPF problems, by exploring the set of solutions in which the maximum loading is restricted by the operational limits of the system, but not by the Hopf bifurcation condition. The

S-OPF problem is solved using the Matlab optimization toolkit, as in the case of CEHB-OPF problem.

The optimization procedure is initialized at the HB point, with the initial set of controllable parameters. The initial HB point is obtained by a sequential Newton-Raphson (SNR) search as discussed for other models. It was observed that it is also possible to initialize the optimization procedure at the initial normal operating point, obtaining the same optimal parameters. This indicates that the problem is not very sensitive to the initial guess. The robustness to initialization is an advantage of the S-OPF problem over the GEHB-OPF and CEHB-OPF problems.

### 3-Bus Test System

The optimization solution for the objective function and the controllable parameters are shown in Table 5.4. The results obtained for the 3-bus test system agree with the exhaustive search results in Section 5.2. The loading margin is improved by 21% as compared to the original system. The eigenvalue movement in the complex plane is the same as what is observed for the previous problems. The optimization procedure took 6 iterations to converge.

Parameter	Original System	Optimal System
$\lambda_{\text{bifurcation}}$	0.284913	0.344709
$ V_1 $ (slack bus)	1.000000	1.100000
$V_{\text{ref}}$ (LTC 1)	1.000000	1.100000

Table 5.4: Optimization results for the ‘3-bus’ test system, when solving the S-OPF problem



### 14-bus Test System

The results obtained for S-OPF problem with the 14-bus test system are equal to those obtained for the CEHB-OPF problem with the same test system, as shown in Table 5.5. The loading margin is improved by 20%. The optimization procedure took 11 iterations to converge.

The real and imaginary components of the critical eigenvalue at the Hopf bifurcation point for the optimal system are:  $\alpha = 0$  and  $\beta = 0.23$ , giving an initial period of oscillation of  $T_0 = \frac{2\pi}{\beta} = 26.18$  seconds. The voltage profile of bus 13 and the eigenvalue movements in the complex plane is the same as the CEHB-OPF problem.

Parameter	Original System	Optimal System
$\lambda_{\text{bifurcation}}$	0.253507	0.305047
$ V_1 $ (slack bus)	1.060000	1.100000
$ V_2 $	1.045000	1.099420
$ V_3 $	1.010000	1.100000
$ V_8 $	1.090000	1.100000
$V_{\text{ref}}$ (LTC 1)	1.000000	1.100000
$P_{\text{gen}}$ (bus 2)	0.400000	0.443783

Table 5.5: Optimization results for the ‘IEEE14bus’ test system, when solving the S-OPF problem

#### 5.3.4 EVI Optimization Problem

The EVI optimization problem is formulated as the minimization of  $\alpha$ , the real component of the critical eigenvalue of the reduced Jacobian matrix, as defined in Section 4.4, satisfying the following conditions: system state equations; algebraic equations; system limits. The loading parameter is set to its normal operating value, rather than the critical value in the previous approaches. The problem is solved using the Matlab optimization toolkit.

The optimization procedure is initialized at the normal operating point, with the initial set of controllable parameters, and with a loading parameter of  $\lambda = 0.1$ . The initial equilibrium point for the given value of  $\lambda$  is computed by a Newton-Raphson (NR) method implemented in Matlab.

### 3-Bus Test System

In the normal operating conditions, the 3-bus test system is stable, that is, all the eigenvalues of the reduced Jacobian matrix of the system have negative real parts. The eigenvalue with the largest real part is a purely real number, given by  $\alpha = -0.2$ .

The optimization procedure took four iterations to converge, and the results are shown in Table 5.6. The value of  $\alpha$  at the normal operating point is optimized to  $\alpha = -0.22$ . A continuation method is used to obtain the maximum loading parameters  $\lambda_{HB}$  of the system for the normal and the optimal values of the controllable parameters. The results are shown in Table 5.7, which also indicates the critical eigenvalue for the maximum loading parameters. It can be noted that, in both cases, the critical eigenvalues are purely imaginary, characterizing the occurrence of Hopf bifurcation at the maximum loading in each case.

As it can be noted in Table 5.7, the maximum loading parameter did not show a significant improvement. An intuitive comprehension of this phenomenon is obtained through the analysis of the eigenvalues movement of the reduced Jacobian matrix for this test system, with respect to the increase in the loading factor, shown in Figure 5.11. As the loading factor increases, the critical eigenvalue of the system is pushed to the left, up to the point where it collides with another real eigenvalue. A pair of complex conjugate eigenvalues is then formed, which moves to the right with

further increases in the loading factor, up to the point where the pair of eigenvalues crosses the imaginary axis at the Hopf bifurcation point. Therefore, this test system exemplifies the fact that a larger EVI does not necessarily correspond to a larger stability margin.

Furthermore, it can be noted that the improvement in the voltage magnitude at the slack bus does not appreciably affect the loading margin of the system when the reference voltage of the LTC transformer remains almost unchanged, Figure 5.12. The observed results agrees with the discussion provided in Section 5.2.

Parameter	Original System	Optimal System
$\alpha$	-0.2	-0.22
$ V_1 $ (slack bus)	1.000000	1.100000
$V_{\text{ref}}$ (LTC 1)	1.000000	1.000544

Table 5.6: Optimization results for the ‘3-bus’ test system, when solving the EVI optimization problem

Parameter	Original System	Optimal System
$\lambda_{\text{HB}}$	0.284951	0.285940
critical eigenvalue	$0 + j 0.38$	$0 + j 0.34$

Table 5.7: Maximum loadability of the system and the corresponding critical eigenvalue, ‘3-bus’ test system, when solving the EVI optimization problem,

### 14-bus Test System

The results of the optimization procedure are shown through Tables 5.8-5.9 and Figures 5.13-5.14. As stated in the previous section for the loading parameter  $\lambda = 0.1$ , the system is in normal operational state and all the eigenvalues of the reduced Jacobian matrix are in the left half-plane of the complex plane (i.e. they have

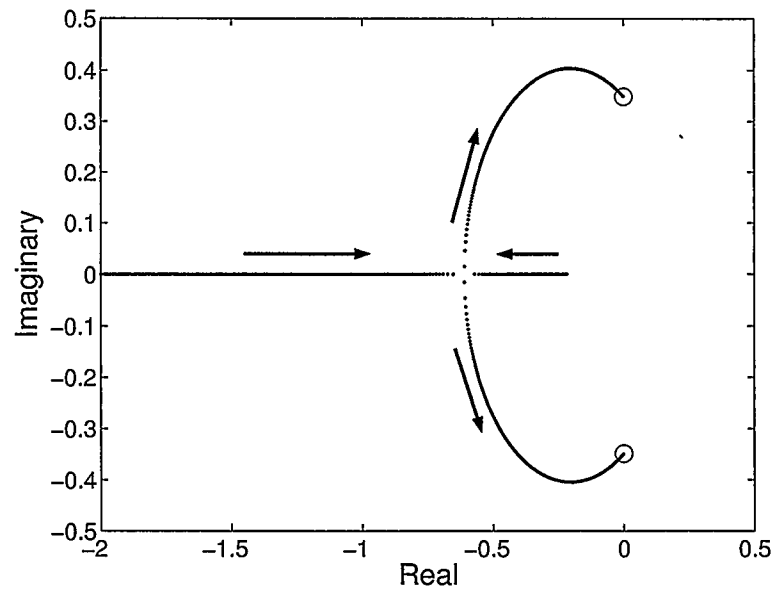


Figure 5.11: Enlargement of the HB region, '3-bus' test system, when solving the EVI optimization problem. Arrows indicate the movement of the two purely real eigenvalues which eventually collide and form a complex conjugate pair. As the value of  $\lambda$  increases the pair move towards the imaginary axis. The point where the complex conjugate pair reach the imaginary axis is shown by circles

negative real parts). The largest eigenvalue for this system is a purely real number, given by  $\alpha = -0.11$ .

The optimization procedure took 10 iterations to converge. Table 5.8 shows the maximum loading parameter for the original and optimal system. As it is shown by the critical eigenvalues both systems experience Hopf bifurcations. However, it was observed that for  $\lambda > 0.101518$  the voltage of bus number 13 drops below the acceptable operational limit for the system with optimal values of the controllable parameters. This is due to the fact that although the magnitude of the voltage at each generator bus is increased for the optimal system, the reference voltage of the LTC transformer is actually decreased, as shown in Table 5.9. Consequently, the magnitude of the voltage at bus 13 drops to 0.9 P.U. for the optimal system. The decrease in the stability margin of the system is illustrated by voltage profile of bus 13 (Figure 5.13). The dotted line in the figure shows the intersection between the lower voltage limit and the voltage profile of bus 13 for the optimal system.

Figure 5.14 shows that the movement of system eigenvalues, with respect to the loading parameter, presents a similar behavior as in the 3-bus test system. Hence, the same reasoning applies when explaining the reduction in the distance to the Hopf bifurcation point, that is, a greater EVI corresponds, in this particular test system, to a smaller loading margin.

Parameter	Original System	Optimal System
$\lambda_c$	0.253596	0.218038
critical eigenvalue	$0 + j 0.23$	$0 + j 0.23$

Table 5.8: Maximum loadability of the system and the corresponding critical eigenvalue, ‘IEEE14bus’ test system, when solving the EVI optimization problem

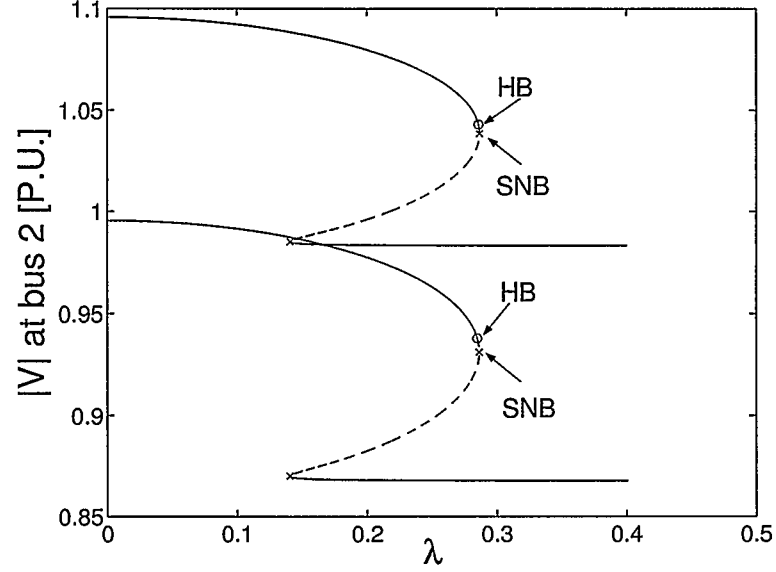


Figure 5.12: Voltage profile of bus 2 in the '3-bus' test system, when solving the EVI optimization problem,

Parameter	Original System	Optimal System
$\alpha$	- 0.11	- 0.16
$ V_1 $ (slack bus)	1.060000	1.100000
$ V_2 $	1.045000	1.100000
$ V_3 $	1.010000	1.100000
$ V_8 $	1.090000	1.100000
$V_{\text{ref}}$ (LTC 1)	1.000000	0.916708
$P_{\text{gen}}$ (bus 2)	0.400000	0.432082

Table 5.9: Optimization results for the 'IEEE14bus' test system, when solving the EVI optimization problem

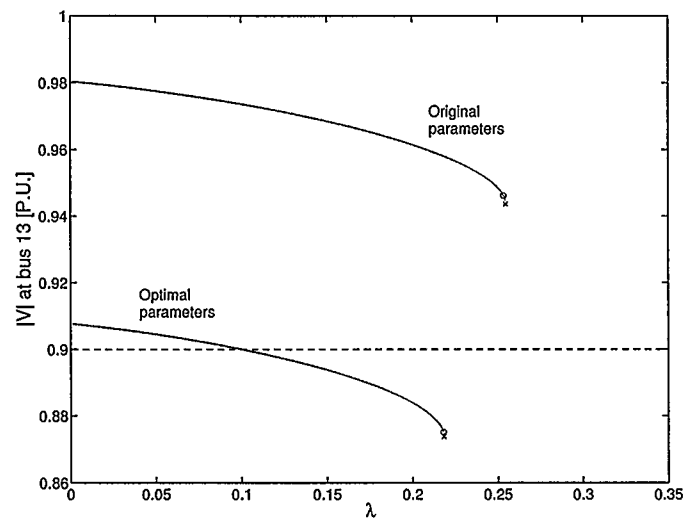


Figure 5.13: Voltage profile of bus 13 in the 'IEEE14bus' test system, when solving the EVI optimization problem. The lower profile represents the system with the optimal values of the controllable parameters and the upper profile is for the original system. The dashed line is used to show the lower voltage limit

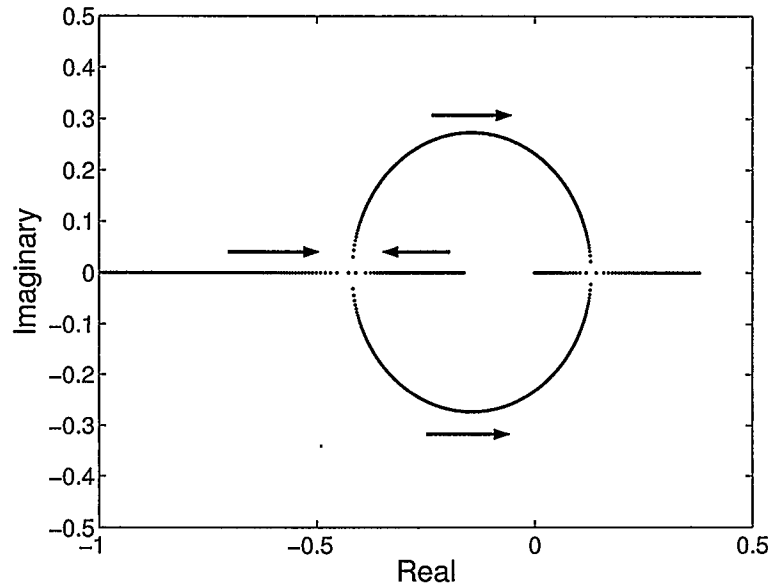


Figure 5.14: Enlargement of the HB region, 'IEEE14bus' test system, when solving the EVI optimization problem. Arrows indicate the movement of the two purely real eigenvalues which eventually crosses the imaginary axis as the value of  $\lambda$  increases

### 5.3.5 SVI Optimization Problem

The SVI optimization problem is formulated as the maximization of the minimum singular value of the modified Jacobian matrix, as defined in Section 4.4.2, satisfying the following conditions: system state equations at rest; algebraic equations; system limits.

The problem is solved using the Matlab optimization toolkit. The optimization procedure is initialized at the normal operating point, with the initial set of controllable parameters, and  $\lambda = 0.1$ , as in the EVI optimization approach. The equilibrium point for given value of  $\lambda$  is found using the NR method. The minimum singular value of the modified Jacobian matrix ( $\mathbf{J}_m$ ) at this point is given by



$$\sigma_{\min} = 0.0201.$$

### 3-Bus Test System

The optimization procedure took 4 iterations to converge. The minimum singular value of matrix  $\mathbf{J}_m$  is optimized to 0.0273. The results are shown in Tables 5.11–5.10 and Figure 5.15.

Table 5.10 shows the improvement of loading margin for optimal system as compared to the original system. Critical eigenvalues indicate that both systems experience Hopf bifurcations at the maximum value of the loading parameter. It can be noted that although the optimal solution of the voltage at the slack bus does not reach the maximum operating limit, the loading margin has improved by 20.7 %.

The increase in the loading margin is exemplified by the voltage profile of bus 2 for the optimal and original system as shown in Figure 5.15. The movement of the eigenvalues in the complex plane is very similar to what was observed for the other problems.

Parameter	Original System	Optimal System
$\lambda_c$	0.2849	0.343931
critical eigenvalue	$0 + j 0.38$	$0 + j 0.45$

Table 5.10: Maximum loadability of the system with the corresponding critical eigenvalue, ‘3-bus’ test system, when solving the SVI optimization problem,

Parameter	Original System	Optimal System
$\sigma_{\min}$	0.201	0.0273
$ V_1 $ (slack bus)	1.000000	1.030195
$V_{\text{ref}}$ (LTC 1)	1.000000	1.100000

Table 5.11: Optimization results for the ‘3-bus’ test system, when solving the SVI optimization problem

### 14-bus Test System

The optimization procedure took 9 iterations to find the optimal solution. Table 5.13 shows the results of the optimization procedure: it is observed that all voltages are increased in a similar manner to that of the CEHB-OPF and S-OPF problems. A continuation method is used to find the maximum loadability of the system for the optimal and original system, which are shown in Table 5.12. An improvement of about 20 % is obtained in the maximum loading parameter of the optimal system compared to the original system. The increase of the loading margin is exemplified using the voltage profile at bus 13, as shown in Figure 5.16. The critical eigenvalue at the maximum  $\lambda$  indicates the occurrence of Hopf bifurcations in both original and optimal systems.

Parameter	Original System	Optimal System
$\lambda_c$	0.253596	0.304075
critical eigenvalue	$0 + j 0.232054$	$0 + j 0.218029$

Table 5.12: Maximum loadability of the system with the corresponding critical eigenvalue, ‘IEEE14bus’ test system, when solving the SVI optimization problem

Parameter	Original System	Optimal System
$\sigma_{\min}$	0.01953	0.0262
$ V_1 $ (slack bus)	1.060000	1.100000
$ V_2 $	1.045000	1.085185
$ V_3 $	1.010000	1.053287
$ V_8 $	1.090000	1.100000
$V_{\text{ref}}$ (LTC 1)	1.000000	1.100000
$P_{\text{gen}}$ (bus 2)	0.400000	0.394286

Table 5.13: Optimization results for ‘IEEE14bus’ test system , when solving the SVI optimization problem

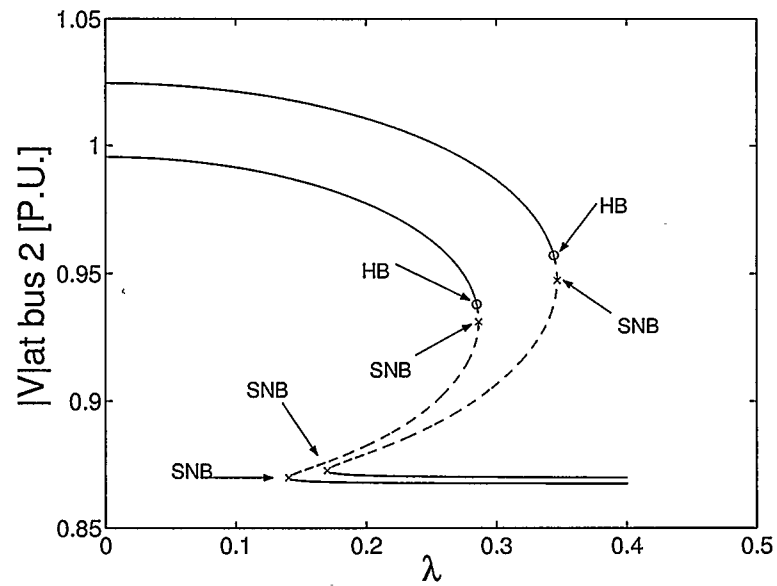


Figure 5.15: Voltage profile of bus 2 in the '3-bus' test system, when solving the SVI optimization problem,

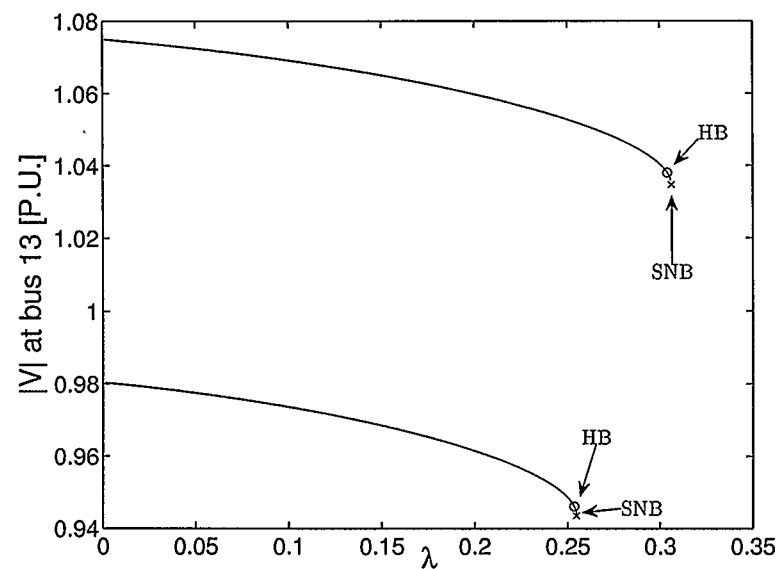


Figure 5.16: Voltage profile of bus 13 in the 'IEEE14bus' test system, when solving the SVI optimization problem, the lower curve indicates the original system and the upper curve represents the optimal system

## 5.4 Comparison of Formulations

In this section all the proposed optimization problems are compared based on their performance, initialization requirements, the possibility of eliminating Hopf bifurcation, and the assumption of a loading direction.

**Performance comparison:** The GEHB-OPF and the EVI optimization problems could not reliably optimize the test systems, as indicated by the following observations:

- The GEHB-OPF problem does not converge for the 14-bus test system. In the 3-bus test system experiment, convergence was achieved to the correct solution (as given by the exhaustive search in Section 5.2), but with a large number of iterations (as compared to the CEHB-OPF, S-OPF, and SVI optimization problems).
- The EVI optimization problem did not effectively improve the stability margin of the 3-bus test system, and the 14-bus test system was made worse than its initial condition.

Therefore, the GEHB-OPF and the EVI optimization problems will be excluded from further comparisons. The remaining optimization problems (CEHB-OPF, S-OPF, and SVI optimization) yield virtually the same performance, as shown in Tables 5.14 and 5.15. The improvement in the maximum system loadability promoted by each optimization problem is approximately the same, and all of the three optimization problems converge in just a few iterations.

**Initialization requirements:** It was noted that the CEHB-OPF problem requires initialization at a bifurcation point. Conversely, the S-OPF and the SVI optimization problems can be initialized at any feasible point.

**Eliminating Hopf bifurcation:** The CEHB-OPF problem has the theoretical disadvantage that it enforces the existence of a Hopf bifurcation at the point of maximum system loadability. In fact, when the operational limits of the system are met before the occurrence of Hopf or saddle-node bifurcation (with respect to the increase in the loading parameter), it is not possible to properly initialize the CEHB-OPF problem: either the operational limit constraints or the Hopf bifurcation constraints would be violated. It must be noted that the S-OPF and the SVI optimization problems do not have this limitation, therefore it is possible to avoid the occurrence of Hopf bifurcation at the maximum loading parameter of the system.

**Loading direction assumption:** Observe that the CEHB-OPF and the S-OPF problems adopt a particular loading direction, namely that of an equal increase in the loading of each machine, given by the loading parameter  $\lambda$ . The SVI optimization problem is less restrictive: since the loading parameter is fixed, there is no assumption of a certain loading direction.

Parameter	GEHB-OPF	CEHB-OPF	S-OPF	EVI	SVI
$\lambda_c$	0.344709	0.344709	0.344709	0.28594	0.34393
loading margin improvement	21%	21%	21%	0.37%	20.7%
iterations	22	6	6	4	4

Table 5.14: Comparison of maximum loading parameter, loading margin improvement, and number of iterations to converge, in all five optimization problem formulations. The test system used is the 3-bus test system.

Parameter	GEHB-OPF	CEHB-OPF	S-OPF	EVI	SVI
$\lambda_c$	—	0.305062	0.305047	0.101518	0.304075
loading margin improvement	—	20%	20%	-60%	20%
iterations	—	13	11	10	9

Table 5.15: Comparison of maximum loading parameter, loading margin improvement, and number of iterations to converge, in all five optimization problem formulations. The test system used is the 14-bus test system. No results were obtained for the GEHB-OPF, since the optimization procedure did not converge.

## 5.5 Summary

In this chapter all the proposed optimization problems are tested using two test systems: a three bus test system, and a 14 bus test system based on IEEE 14 bus standard test case.

It was observed that the GEHB-OPF and EVI optimization problems are not reliable in terms of enhancing the system maximum loadability. The CEHB-OPF, S-OPF and SVI optimization problems showed very similar performance in increasing the system loading margin. Among these methods, the S-OPF and SVI optimization problems are the preferred strategies for maximizing the system loadability, and the choice of which method to apply in a given situation is context dependent. If it is necessary to guarantee the improvement in the loading margin for a given loading direction, the S-OPF problem is preferred. However, if loading direction is not known, the SVI optimization problem can be applied.

## Chapter 6

### Conclusion

This thesis proposes the application of optimization techniques to improve the stability margin of power systems with respect to the occurrence of Hopf bifurcations. In this regard, five optimization problems are formulated in order to compute the optimal values of system variables that yield the maximum system loadability. The effectiveness of the proposed optimization problems is validated using two test systems, and a comparative analysis is presented based on their performance, initialization requirements and assumption of the loading direction.

In Chapter 2, the differential-algebraic model of a power system is presented. The dynamical model of LTC transformers together with a fifth order model of induction motors form the set of differential equations of the system. The algebraic model of the system is formed by the power flow equations and the equations used to connect the induction motors and LTC transformers to the grid.

In Chapter 3, small-disturbance stability analysis is reviewed. Concepts of bifurcation theory are presented, and two types of bifurcations that are often encountered in power system studies are shown: saddle-node and Hopf bifurcations. A discussion on two methods to detect bifurcation in power systems is provided: the usage of indices to predict the occurrence of bifurcation, and the continuation method. The application of optimization theory for system stability analysis is demonstrated by a classical optimal power flow (OPF) problem.

In Chapter 4, five optimization problems are formulated to increase the system

maximum loadability, based on the classical OPF problem, and considering limiting factors such as Hopf bifurcations and operational limits. The OPF problem is modified to incorporate the differential and algebraic equations of induction motors and LTC transformers. The mathematical conditions that define the Hopf bifurcation point are explicitly modeled in the GEHB-OPF, CEHB-OPF, and S-OPF problems, and implicitly modeled in the EVI and SVI optimization problems. The potential advantages and disadvantages of each method are discussed.

In Chapter 5, the proposed optimization problems are tested to assess the validity of the presented formulations. The problems are compared based on their effectiveness to increase the loading margin, initialization and loading direction requirements.

The main contributions of this thesis can be summarized as follows:

- Development of Hopf bifurcation constrained optimal power flow formulations to maximize the system loadability with respect to the Hopf bifurcation (HB) point. The mathematical conditions that define the HB point are included in the OPF problem as constraints. It is assumed that the loading pattern of the system is known. The following optimization problems are proposed:
  1. Generalized Eigenvalue Based Hopf Bifurcation Constrained Optimal Power Flow (GEHB-OPF) problem,
  2. Critical Eigenvalue Based Hopf Bifurcation Constrained Optimal Power Flow (CEHB-OPF) problem,
  3. Stability Constrained Optimal Power Flow (S-OPF) problem.
- Development of optimal power flow problems to maximize an indirect measure of the distance to the Hopf bifurcation point. In this case, the optimal solution



does not guarantee an effective improvement of the system loading margin in a particular direction. The following optimization problems are proposed in this regard:

1. Eigenvalue Index (EVI) optimization problem,
  2. Singular Value Index (SVI) optimization problem.
- Comparative analysis of the proposed models based on the results obtained from the test cases. Furthermore, a discussion of potential advantages and limitations of each method is provided.

It was determined that the S-OPF and the SVI optimization problems yield the best combination of performance and robustness with respect to the initial conditions. The S-OPF problem directly maximizes the distance to bifurcation for a predefined loading direction. The SVI optimization method aims to indirectly enhance the stability margin of the system, through the optimization of the Singular Value Index. Therefore, a loading direction is not required, but the improvement in the loading margin is not guaranteed for all loading directions.

Future directions for the present research include:

- Development of optimization solvers that are specialized for problems with eigenvalue objectives and constraints. Such optimization techniques are a recent and promising research topic in optimization theory [53].
- Extension of the system model to include generator dynamics and other non-linear load models.

## Appendix A

### Solution of Linear Ordinary Differential Equations with Constant Coefficients

Let  $\eta_i \in \mathbb{C}$  be the  $i^{\text{th}}$  eigenvalue of  $\mathbf{J}_{\text{reduced}}$ , and  $\Phi_i \in \mathbb{C}^{D \times 1}$  and  $\Psi_i \in \mathbb{C}^{1 \times D}$  be respectively the right and left eigenvectors of  $\mathbf{J}_{\text{reduced}}$  associated with  $\eta_i$ , that is:

$$\mathbf{J}_{\text{reduced}} \Phi_i = \eta_i \Phi_i \quad (\text{A.1})$$

$$\Psi_i \mathbf{J}_{\text{reduced}} = \eta_i \Psi_i \quad (\text{A.2})$$

where the following relationship holds:

$$\Psi_i \Phi_j = \begin{cases} 1 & \text{for } i = j, \\ 0 & \text{otherwise.} \end{cases}$$

Define the matrix  $\Lambda$  as a diagonal matrix, whose diagonal elements are the eigenvalues of  $\mathbf{J}_{\text{reduced}}$ . Also define the right and left eigenvector matrices as:

$$\Phi = \begin{bmatrix} \Phi_1 & \Phi_2 & \cdots & \Phi_D \end{bmatrix}$$

$$\Psi = \begin{bmatrix} \Psi_1^T & \Psi_2^T & \cdots & \Psi_D^T \end{bmatrix}^T$$

Notice that  $\Psi \Phi = \mathbf{I}$ , therefore  $\Psi = \Phi^{-1}$ . Equations (A.1) and (A.2) can be rewritten in term of matrices  $\Phi$ ,  $\Psi$ , and  $\Lambda$  as:

$$\mathbf{J}_{\text{reduced}} \Phi = \Phi \Lambda$$

$$\Psi \mathbf{J}_{\text{reduced}} = \Lambda \Psi$$

Consider the linearized dynamical system equations as follows:

$$\Delta \dot{\mathbf{x}} = \mathbf{J}_{\text{reduced}} \Delta \mathbf{x} \quad (\text{A.3})$$

Now define an auxiliary vector  $\mathbf{z}$  as:

$$\Delta \mathbf{x} = \Phi \mathbf{z} \quad (\text{A.4})$$

which implies:

$$\mathbf{z} = \Psi \Delta \mathbf{x} \quad (\text{A.5})$$

Observe that (A.4) implies:

$$\Delta \mathbf{x} = \sum_{i=1}^D \Phi_i z_i \quad (\text{A.6})$$

Substituting (A.4) in (A.3), yields:

$$\Phi \dot{\mathbf{z}} = \mathbf{J}_{\text{reduced}} \Phi \mathbf{z} \Leftrightarrow \dot{\mathbf{z}} = \Phi^{-1} \mathbf{J}_{\text{reduced}} \Phi \mathbf{z}$$

Using the fact that  $\Phi^{-1} \mathbf{J}_{\text{reduced}} \Phi = \Lambda$ , the previous equation can be written as  $\dot{\mathbf{z}} = \Lambda \mathbf{z}$ , which yields:

$$z_i(t) = z_i(0) e^{\eta_i t} \quad (\text{A.7})$$

The initial condition  $\mathbf{z}(0)$  can be obtained using (A.5) as:

$$\mathbf{z}(0) = \Psi \Delta \mathbf{x}(0) \Rightarrow z_i(0) = \Psi_i \Delta \mathbf{x}(0) \quad (\text{A.8})$$

Combining (A.6), (A.7), and (A.8) gives the time solution of (A.3):

$$\Delta \mathbf{x}(t) = \sum_{i=1}^D \Phi_i \Psi_i \Delta \mathbf{x}(0) e^{\eta_i t}$$

## Bibliography

- [1] L. Pereira. Cascade to black: Similarities between the 14 august 2003 blackout and the western system collapses of 1996. *IEEE Power & Energy Magazine*, 2(3):54–57, May-June 2004.
- [2] E. Wirth and A. Kara. Innovative power flow management and control technologies. *IEEE Power Engineering*, 14(3):129–140, June 2000.
- [3] Y. R. Sood, N. P. Padhy, and H. O. Gupta. Wheeling of power under deregulated environment of power system—a bibliographical survey. *IEEE Transactions on Power Systems*, 17(3):870–874, August 2002.
- [4] W. D. Rosehart, C. A. Canizares, and V. H. Quintana. Multiobjective optimal power flows to evaluate voltage security costs in power networks. *IEEE Transactions on Power Systems*, 18(2):578–587, May 2003.
- [5] C. Canizares, I. Dobson, Miller N., V. Ajjarapu, H. Hamadanizadeh, and F. Rahimi. *Voltage Stability Assessment: Concepts, Practices and Tools*. IEEE/PES Power System Stability Subcommittee, August 2002. Tech. Rep. SP101PSS.
- [6] Rudiger Seydel. *Practical Bifurcation and Stability Analysis, From Equilibrium to Chaos*. Springer-Verlag, 1994.
- [7] V. Ajjarapu and B. Lee. Bifurcation theory and its application to nonlinear dynamical phenomena in an electrical power system. *IEEE Transactions on Power Systems*, 7(1):424–431, February 1992.

- [8] T. V. Cutsem and C. D. Vournas. *Voltage Stability of Electric Power System*. Kluwer Academic Publishers, 1998.
- [9] P. Kundur, J. Paserba, V. Ajjarapu, G. Andersson, A. Bose, C. Canizares, N. Hatziaargyriou, D. Hill, A. Stankovic, C. Taylor, T. V. Cutsem, and V. Vittal. Definition and classification of power system stability iee/cigre joint task force on stability terms and definitions. *IEEE Transactions on Power Systems*, 19(3):1387–1401, August 2004.
- [10] E. H. Abed and P. P. Varaiya. Nonlinear oscillations in power systems. *International Journal on Electric Power and Energy Systems*, 6(1):37–43, January 1984.
- [11] W. D. Rosehart and C. A. Canizares. Bifurcation analysis of various power system models. *International Journal of Electrical Power and Energy Systems*, 21(3):171–182, March 1999.
- [12] Tan C., Varghese M., Varaiya P., and Wu F. Bifurcation, chaos, and voltage collapse in power systems. In *Proceedings of the IEEE, Invited Paper*, volume 83, pages 1484–1496, November 1995.
- [13] H. G. Kwatny, A. K. Pasrija, and L. Bahar. Static bifurcations in electric power networks: Loss of steady-state stability and voltage collapse. *IEEE Transactions on Circuits and Systems*, 33(10):981–991, October 1986.
- [14] H. G. Kwatny, R. F. Fischl, and C. O. Nwankpa. Local bifurcations in power systems: Theory, computation and application. In *Proceedings of the IEEE, Invited Paper*, volume 83, pages 1456–1483, November 1995.

- [15] V. Venkatasubramanian, H. Schättler, and J. Zaborszky. Local bifurcations and feasibility regions in differential-algebraic systems. *IEEE Transactions on Automatic Control*, 40(12):1992–2013, December 1995.
- [16] R. Chen and P. P. Varaiya. Degenerate hopf bifurcations in power systems. *IEEE Transactions on Circuits and Systems*, 35(7):818–824, July 1998.
- [17] A. A. P. Lerm, C. A. Canizares, and A. S. Silva. Multiparameter bifurcation analysis of the south Brazilian power system. *IEEE Transactions on Power Systems*, 18(2):737–746, May 2003.
- [18] K. Kim, H. Schättler, V. Venkatasubramanian, J. Zaborsky, and P. Hirsch. Methods for calculating oscillations in large power systems. *IEEE Transactions on Power Systems*, 12(4):1639–1648, November 1997.
- [19] C. A. Canizares, N. Mithulananthan, F. Milano, and J. Reeve. Linear performance indices to predict oscillatory stability problems in power systems. *IEEE Transactions on Power Systems*, 19(2):1104–1114, May 2004.
- [20] Z. Y. Dong. Power system security with a parameter space based control scheme. In *Australian Universities Power Engineering Conference*, pages 239–244, September 2001.
- [21] C. P. Gupta, R. K. Varma, and S. C. Srivastava. A method to determine closest hopf bifurcation in power systems considering exciter and load dynamics. In *IEEE Proceedings on Energy Management and Power delivery*, volume 1, pages 293–297, March 1998.

- [22] N. Mithulananthan, C. A. Canizares, J. Reeve, and G. J. Rogers. Comparison of PSS, SVC and STATCOM controllers for damping power system oscillations. *IEEE Transactions on Power Systems*, 18(2):786–792, May 2003.
- [23] Y. V. Makarov, Q. Wu, D. J. Hill, D. H. Popovic, and Z. Y. Dong. Coordinated steady-state voltage stability assessment and control. In *IEEE 4th International Conference on Advances in Power System Control, Operation and Management*, volume 1, pages 248–253, November 1997.
- [24] C. A. Canizares. Calculating optimal system parameters to maximize the distance to saddle-node bifurcations. *IEEE Transactions on Circuits and Systems*, 45(3):225–237, March 1998.
- [25] C. A. Canizares. Applications of optimization to voltage collapse analysis. In *Proceedings of the IEEE/PES Summer Meeting*, San Diego, CA, July 1998.
- [26] N. Mithulananthan and Srivastava S. C. Investigation of a voltage collapse incident in sri lankan power system network. In *IEEE Proceedings of International Conference on EMPD*, volume 1, pages 47–53, March 1998.
- [27] R. Fourer. *AMPL: A Modeling Language for Mathematical Programming*. Thomson/Brooks/Cole, 2nd edition, 2003.
- [28] R. J. Vanderbei. Loqo’s user manual. Technical report, Princeton University, 1997.
- [29] R. J. Vanderbei and D. F. Shanno. An interior-point algorithm for nonconvex

- nonlinear programming. *Computational Optimization and Applications*, 13:231–252, 1999.
- [30] J. Nocedal and S. J. Wright. *Numerical Optimization*. Springer Series in Operations Research. Springer-Verlag, New York, NY, 1999.
- [31] John. J. Grainger and Jr. W. D. Stevenson. *Power System Analysis*. McGraw-Hill Inc., 1994.
- [32] P. Kundur. *Power System Stability and Control*. McGraw-Hill Inc., 1994.
- [33] R. A. Jabr, A. H. Coonick, and B. J. Cory. A primal-dual interior point method for optimal power flow dispatching. *IEEE Transactions on Power Systems*, 17(3):654–662, August 2002.
- [34] A Roguin. Nikola Tesla: The man behind the magnetic field unit. *Journal of Magnetic Resonance Imaging*, 19(3):369–374, 2004.
- [35] Chee-Mun Ong. *Dynamic Simulation of Electric Machinery Using MATLAB/SIMULINK*. Prentice Hall PTR, 1998.
- [36] D. P. S. Gupta and J. W. Lynn. *Electrical Machine Dynamics*. The Macmillan Press Ltd., 1980.
- [37] P. C. Krause, O. Wasynczuk, and S. D. Sudhoff. *Analysis of Electric Machinery and Drive Systems*. IEEE Press and Wiley-Interscience, 1994.
- [38] C. A. Canizares and W. Rosehart. Bifurcation analysis of induction motor loads for voltage collapse studies. In *Proceedings of the North American Power Symposium (NAPS)*, pages 559–565, Boston, MA, November 1996.



- [39] I. Dobson and E. Barocio. Scaling of normal form analysis coefficients under coordinate change. *IEEE Transactions on Power Systems*, 19(3):1438–1444, August 2004.
- [40] A. Kumar and S. C. Srivastava. A zonal congestion management approach using real and reactive power rescheduling. *IEEE Transactions on Power Systems*, 19(1):554–562, February 2004.
- [41] G. H. Golub and C. F. Van Loan. *Matrix Computations*. The John Hopkins University Press, 1993.
- [42] C. A. Canizares, A. C. Z. de Souza, and V. H. Quintana. Comparison of performance indices for detection of proximity to voltage collapse. *IEEE Transactions on Power Systems*, 11(3):1441–1450, August 1996.
- [43] C. A. Canizares, N. Mithulanathan, A. Berizzi, and J. Reeve. On the linear profile of indices for the prediction of saddle-node and limit-induced bifurcation points in power systems. *IEEE Transactions on Circuits and Systems*, 50(12):1588–1595, December 2003.
- [44] I. Dobson. Observations on the geometry of saddle node bifurcation and voltage collapse in electrical power systems. *IEEE Transactions on Circuits and Systems-I: Fundamental Theory and Applications*, 39(3):240–243, March 1992.
- [45] I. Dobson and L. Lu. New methods for computing a closest saddle node bifurcation and worst case load power margin for voltage collapse. *IEEE Transactions on Power Systems*, 8(3):905–913, August 1993.

- [46] C. Alsberg. *WSCC Issues Preliminary Report on August Power Outage: PRESS RELEASE*. WSCC, technical report edition, September 1996. available at <http://www.wsccl.com/augdist.htm>.
- [47] N. Mithulananthan, C. A. Canizares, and J. Reeve. Indices to detect hopf bifurcations in power systems. In *Proceedings of the North American Power Symposium (NAPS)*, Waterloo, ON, October 2000.
- [48] G. L. Torres and V. H. Quintana. An interior-point method for nonlinear optimal power flow using voltage rectangular coordinates. *IEEE Transactions on Power Systems*, 13(4):1211–1218, November 1998.
- [49] J. A. Momoh, M. E. El-Hawary, and R. Adapa. A review of selected optimal power flow literature to 1993 part I: Nonlinear and quadratic programming approaches. *IEEE Transactions on Power Systems*, 14(1):96–104, February 1999.
- [50] I. M. Nejdawi, K. A. Clements, and P. W. Davis. An efficient interior point method for sequential quadratic programming based optimal power flow. *IEEE Transactions on Power Systems*, 15(4):1179–1183, November 2000.
- [51] Y. V. Makarov, Y. D. Zhao, and David J. Hill. A general method for small signal stability analysis. *IEEE Transactions on Power Systems*, 13(3):979–985, August 1998.
- [52] W. D. Rosehart. Stability analysis of detailed power system analysis. Master's thesis, University of Waterloo, September 1997.

- [53] A. S. Lewis. The mathematics of eigenvalue optimization. *Mathematical Programming*, 97(1-2, Series B):155–176, 2003.
- [54] Power systems test case archive. <http://www.ee.washington.edu/research/pstca/>.